different types of myeloid leukemia, we used three types of mouse models of myeloid leukemia induced by the retroviral transduction of granulocyte-monocyte progenitors (GMPs) with MLL-ENL and MOZ-TIF2 and the cotransduction of GMPs with BCR-ABL and NUP98-HOXA9 (Supplemental Figure 1; supplemental material available online with this article; doi:10.1172/JCI68101DS1). LIC-enriched populations of these myeloid leukemia models have been investigated in previous studies: GMP-like leukemia cells (L-GMPs) in MLL-ENL and MOZ-TIF2 models and the lineage$^-$ Sca-1$^+$ fraction in the BCR-ABL/NUP98-HOXA9 model (Supplemental Figure 2, A–C, and refs. 25–27). In order to obtain cell populations that would barely contain LICs, we also sorted lineage$^-$ c-Kit$^-$ cells in MLL-ENL and MOZ-TIF2 leukemic mice and lineage$^+$ cells in a BCR-ABL/NUP98-HOXA9 model. There were striking differences in clonogenic potential (Supplemental Figure 3) and LIC frequencies, as determined by in vivo limiting dilution assays in the two populations of each model (Figure 1A and Supplemental Table 1). Therefore, we confirmed that LIC and non-LIC fractions can be clearly isolated through the surface antigen profiles of the three leukemia models. Next, we visualized the subcellular distribution of the major NF-κB subunit p65 in LICs, non-LICs, and normal cells by immunofluorescence staining and confocal microscopy. As shown in Figure 1B, prominent nuclear translocation of p65 was observed in the LICs of each model, while it was retained mostly in the cytoplasm in normal lineage$^-$ c-Kit$^+$ Sca-1$^+$ cells (KSLs), which are enriched for HSCs and GMPs. Interestingly, non-LICs also had relatively reduced p65 nuclear translocation signal compared with that in LICs in all three leukemia models. We quantified the nucleus/cytoplasm ratio of p65 staining intensity in these images, which also showed that the LICs in each model had significant nuclear localization compared with that observed in non-LICs, normal KSLs, and GMPs (Figure 1C).

To further test NF-κB transcription activity in LICs, we investigated the expression profiles of a subset of genes regulated by the NF-κB pathway. We first used two sets of published gene expression microarray data, which compared the expression profiles of MOZ-TIF2 L-GMPs (26), MLL-AF9 L-GMPs, and HOXA9-MEIS1 L-GMPs (28) with those of normal hematopoietic stem or progenitor cells (HSPCs). The expression profiles of previously identified NF-κB target genes were assessed by gene set enrichment analysis (GSEA) (Supplemental Table 2 and ref. 29), which showed that L-GMPs had increased expression levels of NF-κB target genes compared with those in normal HSPCs in both sets of gene expression microarray data (Figure 2A). We also compared the expression profiles of the same gene set in CD34$^+$CD38$^-$ human AML cells with those of the equivalent cell population in normal BM cells, which corresponded to the HSC fraction, and observed a similar tendency (Figure 2B and ref. 30). Then, we validated these results using quantitative real-time PCR by comparing the expression levels of several NF-κB target genes in LICs and non-LICs from our three mouse models with those in normal GMPs and found increased expression levels of most of the genes in different types of LICs, but no significant elevation of these levels in non-LICs (Figure 2C and Supplemental Figure 4). Furthermore, the level of p65 phosphorylation, which is important for enhancing its transcription activity, was significantly increased in LICs compared with the level observed in normal GMPs (Figure 2D). Consistent with these findings, LICs showed a more prominent increase in apoptosis than did normal cells or non-LICs when treated with sc-514, a selective inhibitor of IκB kinase β (IKKβ) (Figure 2, E and F, and ref. 31). Although LICs from BCR-ABL/NUP98-HOXA9–induced leukemia were rather resistant to sc-514 compared with cells from MLL-ENL– and MOZ-TIF2–induced leukemia, they still showed higher sensitivity than non-LICs. Collectively, these data fully support the hypothesis that the NF-κB pathway is constitutively activated in the LICs of different types of myeloid leukemia.

LICs maintain their constitutive NF-κB activity via autocrine TNF-α signaling. In the next step, we addressed the question of how LICs maintain constitutive NF-κB activity in different types of leukemia models. In order to investigate genes prevalently dysregulated in LICs, we analyzed the previously published microarray-based gene expression profiles comparing murine and human LICs with normal HSPCs (26, 28, 30). After narrowing down our analysis to the genes commonly upregulated in LICs in three different types of murine leukemia models, we further selected nineteen genes whose expression is elevated in human AML CD34$^+$CD38$^-$ cells (Figure 3A). Among the nineteen genes with typically elevated expression levels in LICs, we focused on *Tnf*, because it is well known as an activator of NF-κB and as an NF-κB–regulated gene. For the purpose of directly evaluating TNF-α abundance in the BM of leukemic mice, we measured the concentration of TNF-α in the BM extracellular fluid and confirmed that it was conspicuously enriched in leukemic BM cells compared with normal BM cells (Figure 3B). We also examined the TNF-α concentration in culture media conditioned by LICs, non-LICs, and normal cells, respectively, to determine whether leukemia cells themselves have the ability to secrete TNF-α. We found that TNF-α secretion was distinctly elevated in LICs, while the normal GMP-conditioned media barely included TNF-α (Figure 3C). Although non-LICs also had TNF-α secretory ability, it was much lower that that of LICs. We therefore reasoned that LICs might maintain their NF-κB pathway activity via autocrine TNF-α signaling. To test this hypothesis, we cultured freshly isolated LICs in serum-free media with a TNF-α–neutralizing antibody or its isotype control and observed p65 subcellular distribution. While LICs treated with isotype control antibodies maintained p65 nuclear translocation even after serum-deprived culture, the p65 translocation signal we observed in three types of LICs was significantly attenuated when these cells were cultured with neutralizing antibodies against TNF-α (Figure 3D). The results were also confirmed by quantification of p65 intensity (Figure 3E). These data strongly suggest that different types of LICs have a similarly increased potential for TNF-α secretion, which maintains constitutive NF-κB activity in an autonomous fashion.

Autocrine TNF-α signaling promotes leukemia cell progression. We were then interested in exploring the effect of autocrine TNF-α secretion on leukemia progression. BM cells derived from WT or *Tnf*-knockout mice were transplanted into sublethally irradiated WT recipient mice after transduction with MLL-ENL and MOZ-TIF2, and cotransduction with BCR-ABL and NUP98-HOXA9 (Figure 3F). Although several mice did develop leukemia with prolonged latency, *Tnf*-deficient cells were significantly ($P < 0.01$) impaired in their ability to initiate leukemia (Figure 3G). We confirmed that *Tnf*-deficient LICs show a distinct decrease in nuclear localization of p65 compared with the that in LICs derived from WT BM cells (Supplemental Figure 5, A and B). Next, we examined whether paracrine TNF-α from the BM microenvironment contributes to leukemia progression. When the established leukemia cells were secondarily transplanted into WT or *Tnf*-knockout recipient mice, *Tnf*-deficient leukemia cells failed to effectively establish AML in

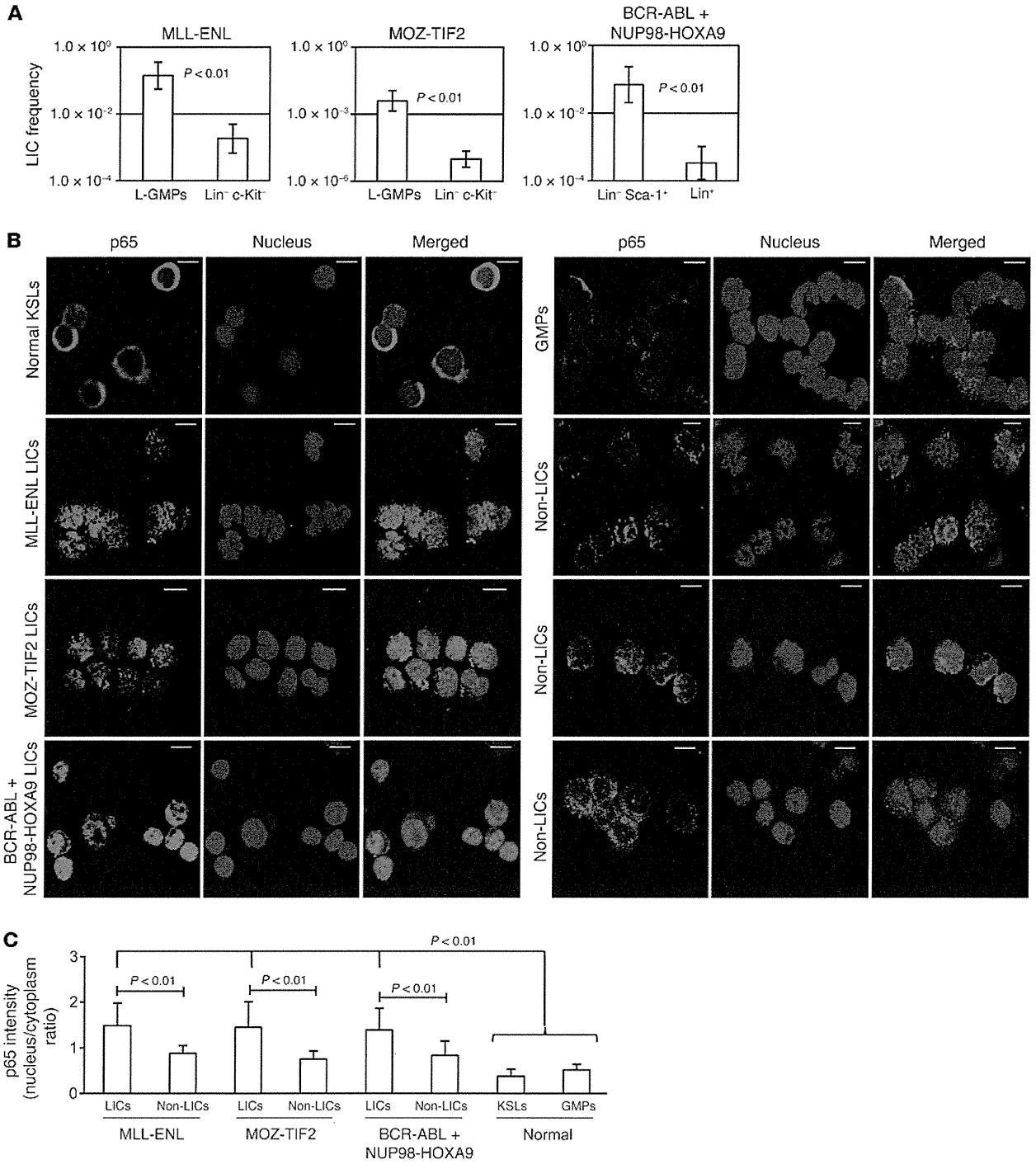

Figure 1

NF-κB pathway is activated in LICs of different murine myeloid leukemia models. (**A**) LIC frequency in the two fractions of each leukemia model as determined by limiting dilution assay. See Supplemental Table 1 for detailed transplantation results. (**B**) Immunofluorescence assessment for p65 nuclear translocation in KSLs, GMPs, LICs, and non-LICs in three leukemia models. Scale bars: 10 μm. (**C**) Quantification of p65 nuclear translocation assessed by the mean nucleus/cytoplasm intensity ratio. More than 50 cells were scored in each specimen, and the average intensity ratio with SD is shown.

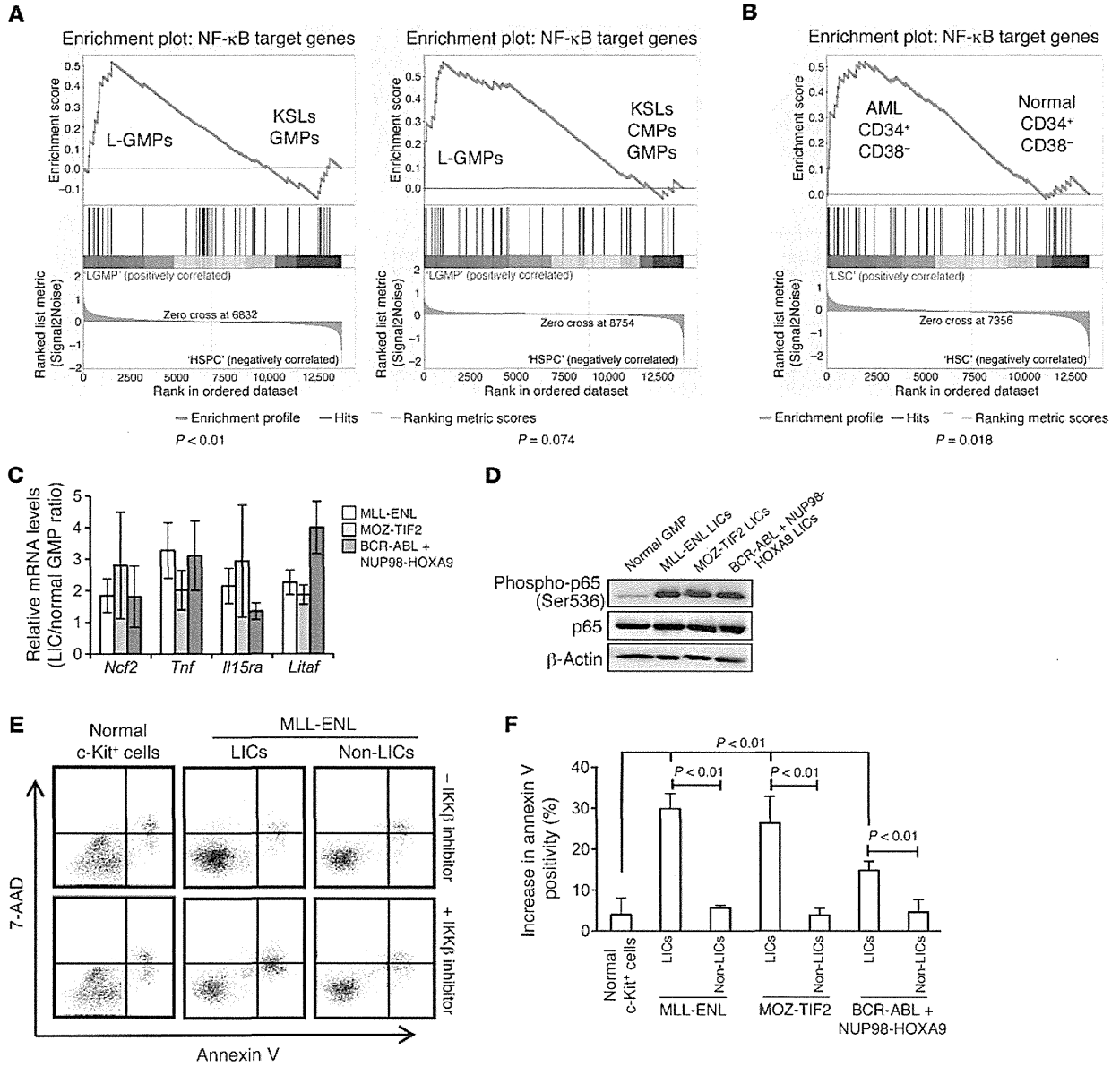

Figure 2

NF-κB transcription activity is increased in LICs. (**A**) GSEA of NF-κB target genes in the published gene expression data comparing LICs in leukemia mouse models with normal HSPCs. Left panel: comparison of MOZ-TIF2 L-GMP with normal KSLs and GMPs (GSE24797). Right panel: comparison of MLL-AF9 and HOXA9-MEIS1 L-GMPs with normal KSLs, common myeloid progenitors (CMPs), and GMPs (GSE20377). (**B**) GSEA of NF-κB target genes in $CD34^+CD38^-$ fractions in human AML versus healthy controls (GSE24006). (**C**) Quantitative real-time PCR analysis of a subset of NF-κB target genes in LICs of MLL-ENL, MOZ-TIF2, and BCR-ABL/NUP98-HOXA9 leukemia models relative to normal GMPs ($n = 4$). Error bars indicate SD. (**D**) Immunoblotting of total and phosphorylated p65 in normal GMPs and LICs in the three leukemia models. (**E**) Representative annexin V and 7-AAD profiles of normal c-Kit+ cells, L-GMPs, and $Lin^-c\text{-}Kit^-$ cells in MLL-ENL leukemic mice after a 24-hour culture with or without 10 μM IKK inhibitor (sc-514). (**F**) Average percentage increase in apoptotic cells in LICs of the three leukemia models compared with that in non-LICs and normal c-Kit+ cells treated with 10 μM IKK inhibitor (sc-514) ($n = 4$ each). Error bars indicate SD.

all three models (Figure 3, H and I). Interestingly, there was no significant difference in leukemogenicity among the recipient genotypes. These results indicate that autocrine TNF-α secretion is important for AML progression and that the contribution of paracrine effects derived from stromal cells is minimal.

The impact of specific NF-κB inhibition on leukemia progression. To investigate the influence of specific NF-κB pathway inhibition on leukemia progression in vivo, we transduced MLL-ENL leukemia cells with a retroviral vector expressing a dominant-negative form of IκBα (super repressor, referred to herein as IκB-SR) or

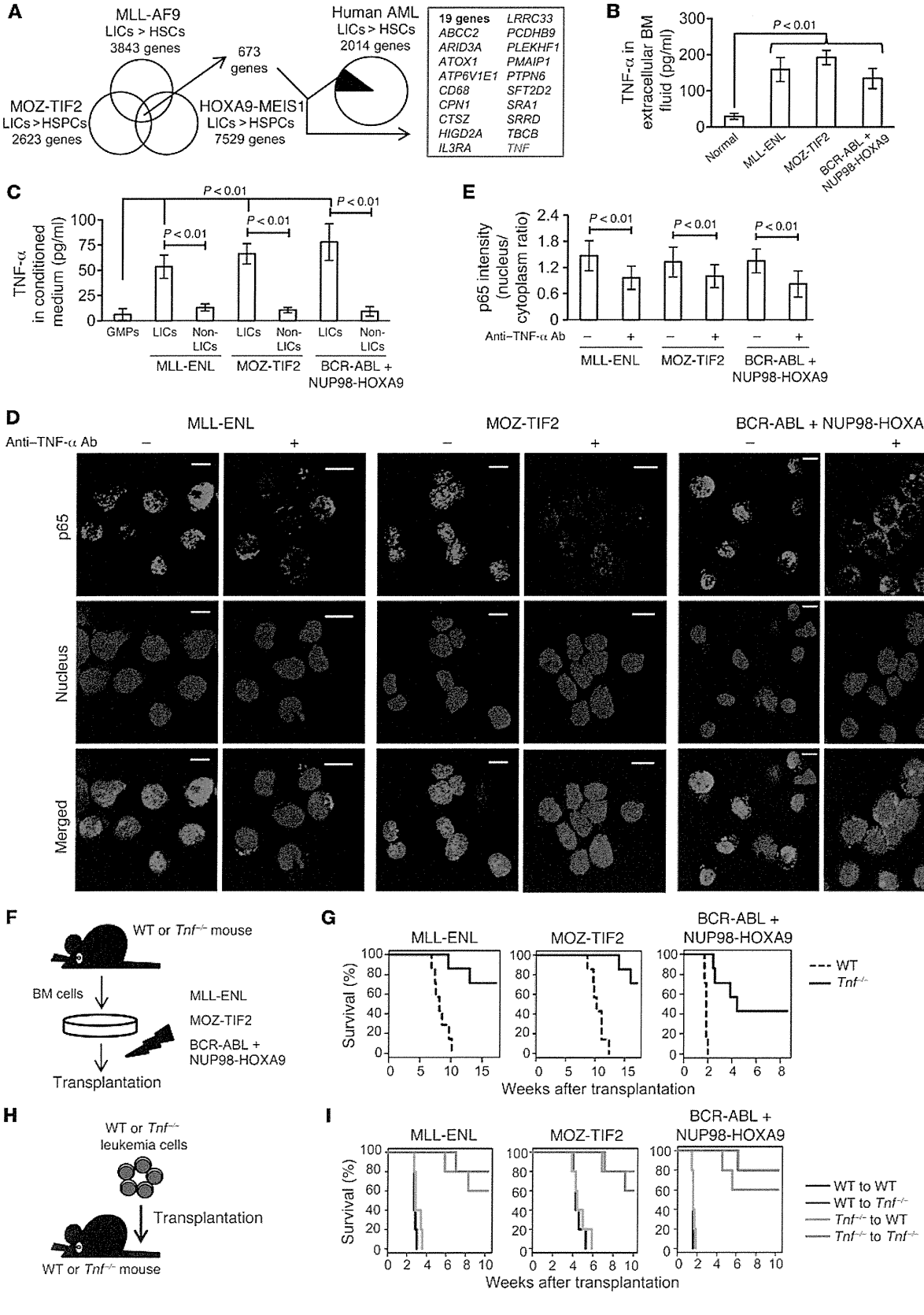

Figure 3
Autocrine TNF-α secretion maintains constitutive NF-κB activity and confers proliferative advantage in LICs. (**A**) Thorough investigation of genes with elevated expression in murine and human LICs compared with that in normal HSPCs in the published gene expression data. (**B**) TNF-α ELISA in extracellular fluid of normal or leukemic BM (n = 4 each). Error bars indicate SD. (**C**) TNF-α secretory ability in LICs compared with that of non-LICs and normal GMPs assessed by ELISA in cultured media (n = 4 each). Error bars indicate SD. (**D**) Immunofluorescence assessment for p65 nuclear translocation in LICs in serum-free culture medium with neutralizing antibody against TNF-α or isotype control. Scale bars: 10 μm. (**E**) Quantification of p65 nuclear translocation of LICs treated with neutralizing antibody against TNF-α or isotype control assessed by the mean nucleus/cytoplasm intensity ratio. More than 50 cells were scored in each specimen, and the average intensity ratio with SD is shown. (**F**) Schematic representation of the experiments. BM cells derived from WT or *Tnf*-knockout mice were transduced with MLL-ENL, MOZ-TIF2, and BCR-ABL plus NUP98-HOXA9 and transplanted into sublethally irradiated mice. (**G**) Survival curves of mice in the experiments shown in **F** (n = 7 each). (**H**) Schematic representation of the experiments. WT or $Tnf^{-/-}$ leukemia cells were secondarily transplanted into WT or $Tnf^{-/-}$ recipient mice. (**I**) Survival curves of mice in the experiments shown in **H** (n = 5 each).

with a control vector, transplanted them into recipient mice, and compared the characteristics of the repopulating cells (Figure 4A). Although the introduction of IκB-SR did not affect the morphology of MLL-ENL leukemia cells (Supplemental Figure 6A), p65 was almost completely sequestered in the cytoplasm of L-GMPs with IκB-SR (Figure 4B and Supplemental Figure 6B), and the expression levels of NF-κB target genes, including *Tnf*, were substantially decreased (Figure 4C). Considering that the blockage of autocrine TNF-α attenuated NF-κB signaling, we hypothesized that NF-κB activity and TNF-α secretion form a positive feedback loop in LICs. We therefore established MOZ-TIF2 and BCR-ABL/NUP98-HOXA9 leukemia cells with IκB-SR. The introduction of IκB-SR significantly decreased a proportion of the cells in the S and G2/M phases of the cell cycle and resulted in a substantial growth delay of those cells in liquid culture (Supplemental Figure 6, C and D). Moreover, leukemia cells with IκB-SR had a reduced colony-forming capacity, while the transduction of IκB-SR into normal HSCs had no significant influence on their colony-forming ability (Figure 4D). Finally, we transplanted leukemia cells with IκB-SR into sublethally irradiated mice and observed a remarkable delay in leukemia progression (Figure 4E). We also confirmed that the developed leukemia cells with IκB-SR had reduced nuclear translocation of p65 compared with that seen in control cells (Supplemental Figure 6E). In contrast, when normal BM cells were transduced with IκB-SR and transplanted into lethally irradiated mice, we observed no significant differences in the reconstitution capacity of the transplanted cells, nor did we find significant differences in peripheral blood cell counts or PBL surface-marker profiles, indicating that NF-κB pathway inhibition exerts a marginal influence on normal hematopoiesis (Supplemental Figure 7, A–C). Collectively, these findings clearly demonstrate that enhanced NF-κB activity in LICs plays a supportive role in leukemia progression and that NF-κB inhibition severely attenuates the proliferative ability of these cells.

To further validate the importance of the NF-κB pathway in leukemia progression, we used BM cells from $Rela^{flox/flox}$ mice (32). We similarly established leukemia cells derived from $Rela^{flox/flox}$ BM cells. Then, the developed leukemia cells were infected with codon-improved Cre recombinase–IRES-GFP (iCre-IRES-GFP) or GFP empty vector, and GFP-positive cells were isolated and secondarily transplanted into sublethally irradiated mice (Figure 4F). Remarkably, most of the mice transplanted with *Rela*-deleted leukemia cells did not develop leukemia (Figure 4G). Compared with controls, several mice did develop leukemia after longer latencies, but they did not develop leukemia after tertiary transplantation (data not shown), indicating that the complete ablation of NF-κB drastically reduced leukemogenicity.

High proteasome activity in LICs yields differences in NF-κB activity between leukemia cell populations. We next sought to elucidate the mechanisms underlying the differences in p65 nuclear translocation status between LICs and non-LICs. We confirmed that LICs had substantially lower IκBα protein levels compared with those of non-LICs in all three models (Figure 5, A and B). These results are very consistent with the p65 distribution status of LICs and non-LICs, considering that NF-κB is usually sequestered in the cytoplasm, bound to IκBα, and translocates to the nucleus, where IκBα is phosphorylated and degraded upon stimulation with a variety of agents such as TNF-α (33). We initially tested whether the expression of IκBα is downregulated in LICs at the transcription level and found that LICs had a tendency toward increased *Nfkbia* mRNA expression levels compared with non-LICs (Figure 5C). Moreover, when *Nfkbia* mRNA translation was inhibited by treatment with cycloheximide, the reduction in IκBα protein levels was more prominent in LICs than in non-LICs (Figure 5, D and E). These data indicate that the differences in IκBα levels are caused by the protein's predominant degradation in LICs. Since both LICs and non-LICs are similarly exposed to high levels of TNF-α within leukemic BM cells, we considered that there would be differences in response to the stimulus and sequentially examined the downstream signals. We first hypothesized that there is a difference in TNF-α receptor expression levels between LICs and non-LICs that leads to greater TNF-α signal transmission in LICs. The expression patterns of TNF receptors I and II were, however, almost similar in LICs and non-LICs, although they varied between leukemia models (Supplemental Figure 8A). We next tested the phosphorylation capacity of IκB kinase (IKK) by examining the ratio of phosphorylated IκBα to total IκBα after treatment with the proteasome inhibitor MG132. Contrary to our expectation, a similar accumulation of the phosphorylated form of IκBα was seen in both LICs and non-LICs, implying that they had no significant difference in IKK activity (Supplemental Figure 8B). Another possibility is that the differences in IκBα protein levels are caused by predominant proteasome activity in LICs, because it is required for the degradation of phosphorylated IκBα. We measured 20S proteasome activity in LICs and non-LICs in each leukemia model by quantifying the fluorescence produced upon cleavage of the proteasome substrate SUC-LLVY-AMC and observed a 2- to 3-fold higher proteasome activity in LICs (Figure 5F). Furthermore, the expression of several genes encoding proteasome subunits was elevated in LICs compared with that in non-LICs (Figure 5G). Similarly, the published gene expression data on human AML samples revealed that $CD34^+CD38^-$ cells had increased expression levels of proteasome subunit gene sets compared with those in $CD34^-$ cells (Supplemental Figure 9 and ref. 30). These findings suggest that enhanced proteasome activity in LICs leads to more efficient degradation of IκBα in response to TNF-α, thus resulting in elevated NF-κB activity. We then tested the effect of bortezomib, a well-

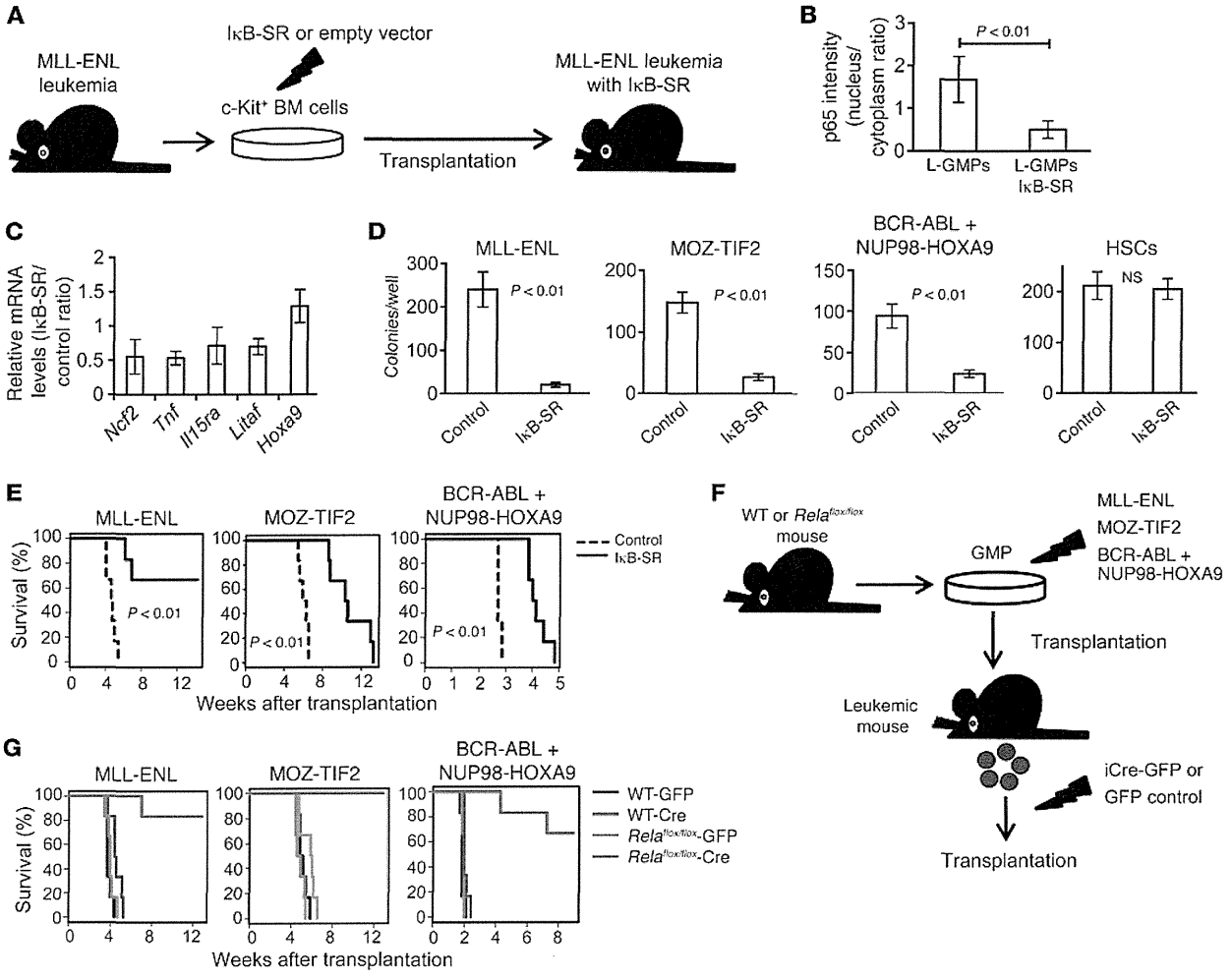

Figure 4

Specific inhibition of NF-κB significantly inhibits leukemia progression in vivo. (**A**) Schematic representation of the following experiments: c-Kit+ BM cells isolated from MLL-ENL leukemic mice were transduced with IκB-SR or control vector and transplanted into sublethally irradiated mice. (**B**) Quantification of p65 nuclear translocation assessed by the mean nucleus/cytoplasm intensity ratio by immunofluorescence staining. More than 50 cells were scored in each specimen, and the average intensity ratio with SD is shown. (**C**) Relative expression profiles of NF-κB target genes in MLL-ENL leukemia cells with or without IκB-SR. The change in *Hoxa9* expression is shown as a control gene not regulated by NF-κB. Error bars indicate SD (n = 3 each). (**D**) CFC assay of leukemia cells and normal HSCS with or without IκB-SR. Cells were seeded at 2,000 cells per well in MLL-ENL or BCR-ABL/NUP98-HOXA9–induced leukemia cells, at 500 cells per well in MOZ-TIF2–induced leukemia cells, and at 1,000 cells per well in normal HSCs (n = 6 in each experiment). (**E**) Survival curves of mice transplanted with MLL-ENL, MOZ-TIF2, and BCR-ABL/NUP98-HOXA9 leukemia cells with or without IκB-SR (n = 6 each). (**F**) Schematic representation of the following experiments: WT or *Rela*$^{flox/flox}$ mice were transduced with MLL-ENL, MOZ-TIF2, or BCR-ABL plus NUP98-HOXA9 and transplanted into sublethally irradiated mice. The developed leukemia cells were transduced with iCre-IRES-GFP or control GFP, and GFP+ cells were secondarily transplanted into mice. (**G**) Survival curves of mice in the experiments shown in **F** (n = 6 each).

known proteasome inhibitor, on LICs in vivo (Figure 5H). First, we treated mice with full-blown leukemia with a single injection of bortezomib and compared their BM surface-marker profiles with those of the vehicle-treated mice. Notably, bortezomib-treated mice showed a significant decrease in LIC-enriched populations in each type of leukemia (Figure 5, I and J). Finally, we treated mice with bortezomib after LIC transplantation and observed significant improvement in survival in those treated with bortezomib (Figure 5K). These results are very consistent with the selectively elevated proteasome activity we observed in LICs.

Enforced activation of the NF-κB pathway increases LIC frequency in leukemic BM. Given the supportive role of the NF-κB pathway in LIC proliferation as well as the differences in its activation status observed between LICs and non-LICs, we reasoned that the attenuation of NF-κB activity might be related to the transition from LICs to non-LICs. To test this hypothesis, we transduced MLL-ENL leukemia cells with a retrovirus encoding shRNA against IκBα and transplanted them into sublethally irradiated mice (Figure 6A). Because IκBα works as an inhibitor of NF-κB by holding it in the cytoplasm, its downregulation should function to

enhance NF-κB activity, regardless of the basal proteasome activity. We first confirmed that MLL-ENL leukemia cells with shRNA-mediated knockdown of IκBα (MLL-ENL-IκBα^{KD}) showed decreased IκBα protein levels in the cytoplasm and increased nuclear p65 protein levels, which would indicate that NF-κB signal was enhanced by the reduction of its cytoplasmic inhibitor (Figure 6B). In accordance with this finding, MLL-ENL-IκBα^{KD} cells had a significantly greater ability to secrete TNF-α than did control cells, reflecting an activated NF-κB/TNF-α signaling loop (Figure 6C). We further investigated the phenotype of leukemic mice with MLL-ENL-IκBα^{KD}. Interestingly, the BM of these MLL-ENL-IκBα^{KD} mice showed a marked increase in immature Gr-1^{lo} c-Kit^{hi} cell populations (Figure 6D). Consistent with this change, we found that these leukemic cells had a greater CFC capacity (Figure 6E). Additionally, in order to investigate the frequency of LICs in BM mononuclear cells, we performed limiting dilution analysis by secondary transplantation of leukemia cells. Although the disease latency for leukemia development was not significantly different among the leukemia cells, MLL-ENL-IκBα^{KD} leukemia cells had a marked abundance of LICs in the leukemic BM mononuclear cells compared with the control shRNA cells (Figure 6F and Supplemental Figure 10A). These data indicate that enforced NF-κB activation expands the LIC fraction in MLL-ENL leukemic BM cells. We also transduced normal BM cells with shRNAs against IκBα and transplanted them into lethally irradiated mice to test whether NF-κB activation by itself can induce leukemia or myeloproliferative-like disease. Over the 4-month follow-up period, the mice exhibited no significant change in peripheral blood values, indicating that NF-κB signal alone is not sufficient for leukemogenesis (Supplemental Figure 10B).

Significant correlation between NF-κB and TNF-α is observed in human AML LICs. Finally, we investigated NF-κB/TNF-α positive feedback signaling in human AML LICs. We analyzed CD34$^+$ CD38$^-$ cells derived from 12 patients with previously untreated or relapsed AML and the same cell population from 5 normal BM specimens (Table 1) and evaluated their NF-κB signal intensity. We also quantified the concentration of TNF-α in the culture media conditioned by CD34$^+$CD38$^-$ cells from each patient in order to measure the TNF-α secretory ability of these cells. As expected, our data from both of these analyses showed a wide variation among patients, one that might reflect a heterogeneous distribution and frequency of the LIC fraction in human AML cells, as was previously described (23). LICs in most of the patients did, however, show increased p65 nuclear translocation and TNF-α secretory potential compared with normal HSCs (Figure 7, A and B, and Supplemental Figure 11). We plotted these two parameters for each patient to compare between patients. Interestingly, a significant positive correlation was demonstrated statistically (P = 0.02), as LICS with enhanced p65 nuclear translocation showed a tendency toward abundant TNF-α secretion (Figure 7C). We also compared p65 intensity between LICs and non-LICs in 2 patients (patients 1 and 3) and found that p65 nuclear translocation was predominant in LICs, which is also consistent with the data obtained in murine AML cells (Supplemental Figure 11). Moreover, we cultured LICs with or without neutralizing antibodies against TNF-α and assessed p65 nuclear translocation to determine the effect of autocrine TNF-α on NF-κB activity. When incubated in the presence of TNF-α–neutralizing antibodies, nuclear translocation of p65 was significantly suppressed in LICs (Figure 7, D and E). These results support our hypothesis that a positive feedback loop exists between NF-κB and TNF-α in human AML LICs.

Discussion

In the present study, we provide evidence that LICs, but not normal HSPCs or non-LIC fractions within leukemic BM, exhibit constitutive NF-κB pathway activity in different types of myeloid leukemia models. Moreover, we identified the underlying mechanism involved in the maintenance of this pathway activity, which had yet to be elucidated. We found that autocrine TNF-α secretion, with the support of enhanced proteasome activity, contributed to a constitutive activation of the NF-κB pathway in LICs. Although we observed different sensitivities to the inhibition of these signaling cascades according to the type of leukemia, these cascades play an important role in LIC proliferation, especially considering that the complete ablation of *Tnf* or *Rela* distinctly suppressed leukemia progression in vivo. These findings, which we validated in human AML LICs, could translate into improved AML treatment strategies.

The strong connection between inflammation and cancer has been increasingly discussed, and the NF-κB pathway is now recognized as a major regulator bridging the two pathological conditions in different types of malignancies. In most of these malignancies, aberrant activation of the NF-κB pathway derives from inflammatory microenvironments that are mainly created by proinflammatory immune cells such as tumor-infiltrating macrophages, neutrophils, and lymphocytes (34, 35). In this study, however, LICs retained their p65 nuclear translocation even after serum-free culture, suggesting that the constitutive NF-κB activity of LICs is maintained in an autonomous fashion. Through our investigation of gene expression profiles in LICs and normal HSCs, we found that LICs had distinctly elevated TNF-α expression levels that contributed to the maintenance of NF-κB activation in LICs. Conversely, the introduction of IκB-SR markedly suppressed TNF-α expression levels, indicating that NF-κB activity and TNF-α secretion create a positive feedback loop in LICs. Moreover, our hypothesis is strongly supported by our findings that a positive correlation exists between NF-κB and TNF-α secretory activities in human AML CD34$^+$CD38$^-$ cells and that inhibition of autocrine TNF-α signaling attenuates p65 nuclear translocation. The role of TNF-α in the process of tumor promotion has recently been demonstrated in various types of solid tumors (36–39). It has also been reported that TNF-α is required for clonal evolution of myeloid malignancies (40). On the other hand, there has been controversy over the effect of TNF-α on leukemia cells when it was exogenously administered (41, 42). However, these previous studies did not address the critical question of whether endogenously secreted TNF-α is required for the maintenance of established leukemia cells, which is a crucially important aspect when considering therapeutic applications. We clearly reveal that the autonomously secreted TNF-α had beneficial effects on LIC proliferation through NF-κB activation, while the contribution of paracrine TNF-α secretion from BM microenvironments was minimal. Another important aspect of cytokine secretion by LICs that was not investigated in the present study is whether this secretion can exert some influence on BM stromal cells. Since the importance of bidirectional crosstalk between leukemia and niche cells through a variety of cytokines has increasingly been recognized (43), TNF-α secreted from LICs might also modulate the function of BM stromal cells, which could also have an impact on leukemia

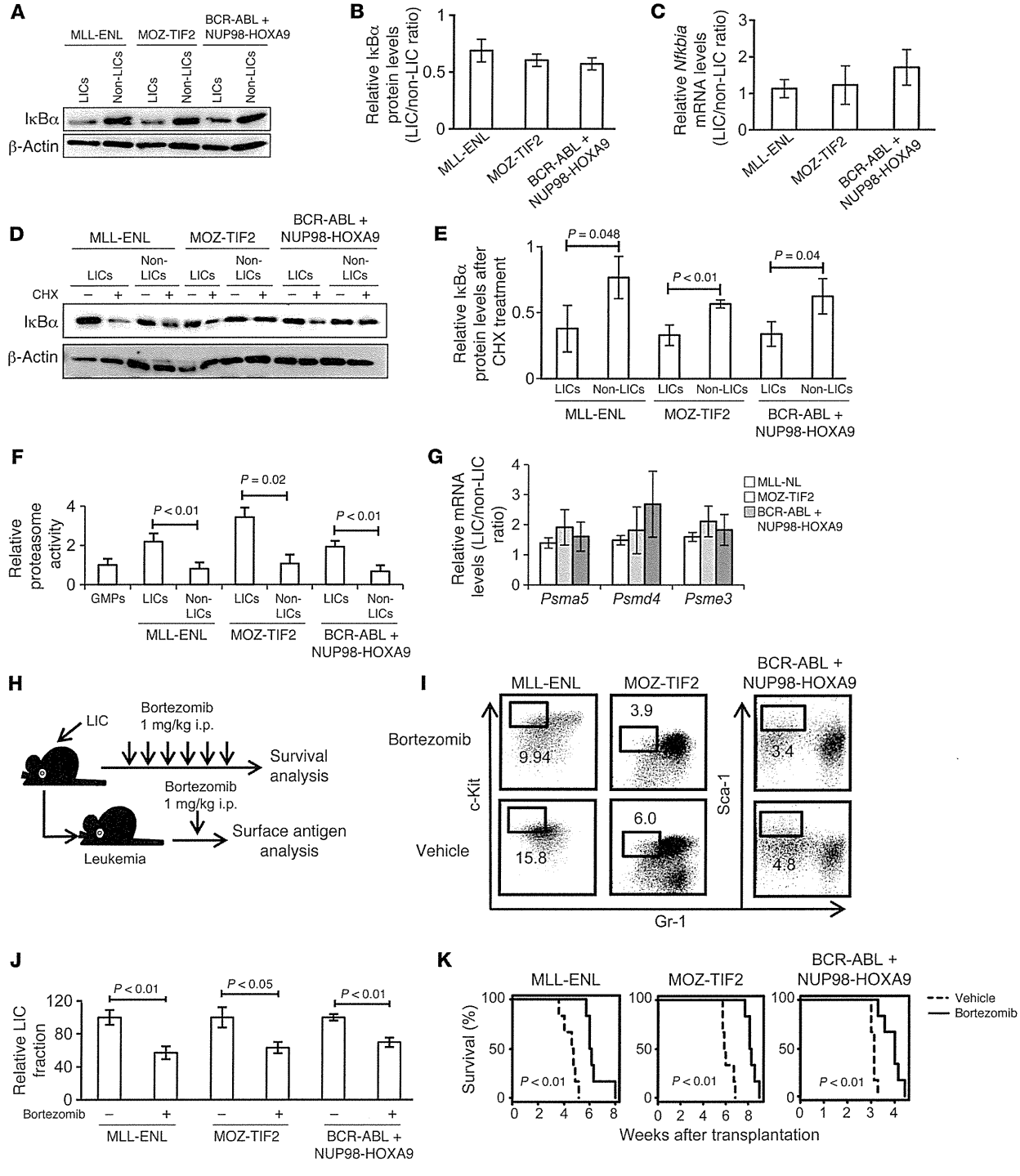

Figure 5
LICs have higher proteasome activity than non-LICs. (**A** and **B**) Immunoblotting of IκBα in LICs and non-LICs (**A**). Protein levels were quantified with ImageJ software (**B**). Data representative of four experiments with SD are shown. (**C**) Relative mRNA expression of *Nfkbia* in LICs compared with that in non-LICs ($n = 4$ each). Error bars indicate SD. (**D** and **E**) Immunoblotting of IκBα in LICs and non-LICs. Cells were pretreated with MG132 for 1 hour and incubated for an additional hour with or without cycloheximide (CHX) (**D**). IκBα protein levels were quantified with ImageJ software, and the relative decrease in IκBα after cycloheximide treatment was calculated ($n = 3$ each). Error bars indicate SD (**E**). (**F**) Analysis of 20S proteasome activity quantified with fluorescence produced upon cleavage of the proteasome substrate SUC-LLVY-AMC ($n = 4$ each). Error bars indicate SD. (**G**) Relative mRNA expression of proteasome subunits in LICs compared with that in non-LICs ($n = 4$ each). Error bars indicate SD. (**H**) Schematic representation of the experiments. Each type of LIC was secondarily transplanted into mice. Bortezomib was injected twice weekly or injected once after incidence of leukemia. (**I** and **J**) Comparison of surface marker profiles in leukemic mice treated with bortezomib or vehicle. Representative FACS data (**I**) and relative percentages of Gr-1^{lo} c-Kit^{hi} fraction in MLL-ENL– or MOZ-TIF2–induced leukemic mice, and Gr-1^{lo}Sca-1^{hi} fraction in BCR-ABL/NUP98-HOXA9–induced leukemic mice are shown ($n = 3$ each) (**J**). Values of control mice were normalized to 100%. Error bars indicate SD. (**K**) Survival curves of mice in the experiments shown in **H** ($n = 6$ each).

progression. Unveiling the role of TNF-α as a paracrine mediator would further extend the therapeutic options for AML.

Few studies have compared the NF-κB activity of different fractions within leukemia cells, and the mechanism underlying the difference in this activity has not been analyzed (44). We focused on proteasome activity as the essential machinery supporting NF-κB activity in LICs. Although high proteasome activity has been reported in various types of cancers (45, 46), its actual role in the malignant phenotype remained to be elucidated. In this study, we found that proteasome activity was especially high in LICs, which contributed to selective NF-κB activity in LICs via the efficient degradation of IκBα. Conversely, the inefficient NF-κB nuclear translocation we observed in non-LICs, despite TNF-α–enriched leukemic BM cells, could be explained by the low proteasome activity in these cells. Therefore, we postulate that both an activating stimulus such as TNF-α and high proteasome activity are required for efficient NF-κB signaling (Figure 7F). Both of these conditions are present exclusively in LICs, which acquire selective NF-κB activation. We also found that the expression levels of proteasome subunit genes were elevated in LICs compared with those in non-LICs, genes that could be involved in regulating proteasome function. Because we observed similar expression patterns in LICs and non-LICs in human AML cells, an elevated expression level of proteosome subunit genes might be one of the common characteristics of the LIC phenotype. Further studies will be needed to elucidate the regulatory mechanism of the proteasome gene families.

Our findings provide several advantages when considering their application to the clinical care setting. First, an activated NF-κB/TNF-α feedback loop was seen in AML LICs that had different genetic abnormalities. Although the therapeutic strategy of targeting aberrant molecules based on genetic abnormalities such as FLT3-ITD is promising, its application is limited to a particular group of patients. In contrast, inhibition of the NF-κB signal in addition to standard chemotherapy would show beneficial effects in most AML patients. Second, because there was a strong positive correlation between the NF-κB signal and TNF-α secretion, therapeutic efficacy could easily be inferred from the abundance of TNF-α instead of from evaluation of the activation status of NF-κB. Third, the NF-κB/TNF-α signal and enhanced proteasome activity are selectively seen in LICs, but not in normal HSCs. A recent study has shown that complete ablation of p65 in hematopoietic cells attenuates the long-term capacity for hematopoietic reconstitution (47). However, our data from the experiments in which we introduced IκB-SR into normal BM cells show that partial repression of NF-κB activity exerted minimal influence on normal hematopoiesis, while it markedly inhibited leukemia progression. These results indicate that there is a therapeutic window during which LICs can selectively be killed by NF-κB inhibition without seriously affecting normal hematopoiesis. Alternatively, there is some evidence that TNF-α has suppressive effects on normal HSCs (48, 49). The opposing role of TNF-α in LICs and HSCs is additionally beneficial, since anti–TNF-α therapy contributes to the recovery of normal hematopoiesis and attenuates LIC proliferation. Now that the TNF-α antagonist etanercept is widely used in inflammatory diseases such as rheumatoid arthritis, this drug might be a promising candidate for treating patients with AML.

In summary, the present study shows that blocking the NF-κB pathway offers a promising therapeutic approach for targeting LICs in various types of myeloid leukemia, without disturbing normal hematopoiesis. We further determined that autocrine TNF-α signaling and enhanced proteasome activity are crucial for maintaining constitutive NF-κB activity in LICs, findings that may also provide a new therapeutic opportunity.

Methods

Animals. C57BL/6 mice and BALB/c mice were purchased from Japan SLC, Inc. *Tnf*-knockout mice on a BALB/c background were established as described previously (50). *Rela*-floxed mice on a C57BL/6 background were provided by H. Algül and R.M. Schmid (32). BALB/c mice were used as the controls in the experiments using *Tnf*-knockout mice, and C57BL/6 mice were used in the other experiments.

Retrovirus production and BM transplantation assays. To obtain retrovirus supernatants, platinum-E (Plat-E) packaging cells were transiently transfected with each retrovirus vector, and the viral supernatants were collected 48 hours after transfection and used immediately for infection. To establish each myeloid leukemia mouse model, we used pMSCV-neo-MLL-ENL; pMSCV-MLL-ENL–internal ribosome entry site–*EGFP* (*IRES-EGFP*); pGCDNsam-MLL-ENL-*IRES*-Kusabira-Orange; pGCDNsam-MOZ-TIF2-*IRES-EGFP*; pGCDNsam-MOZ-TIF2-*IRES*-Kusabira-Orange; pGCDNsam-BCR-ABL-*IRES-EGFP*; pGCDNsam-BCR-ABL-*IRES*-Kusabira-Orange; and pMSCV-neo-NUP98-HOXA9. GMPs isolated from the BM of 8- to 10-week-old mice were transduced with the respective vectors and injected into sublethally irradiated (7.5 Gy) recipient mice. For experiments involving the generation of leukemia cells with IκB-SR, MLL-ENL leukemia cells were transduced with pBabe-GFP or pBabe-GFP-IκB-SR. MOZ-TIF2, and BCR-ABL/NUP98-HOXA9 leukemia cells were transduced with pGCDNsam-Kusabira-Orange or pGCDNsam-IκB-SR-IRES-Kusabira-Orange. For experiments involving the deletion of p65 in *Rela*-floxed mice, leukemia cells were established using Kusabira-Orange–containing retroviral vectors. The developed leukemia cells were transduced with pGCDNsam-EGFP or pGCDNsam-iCre-EGFP and transplanted into sublethally irradiated mice.

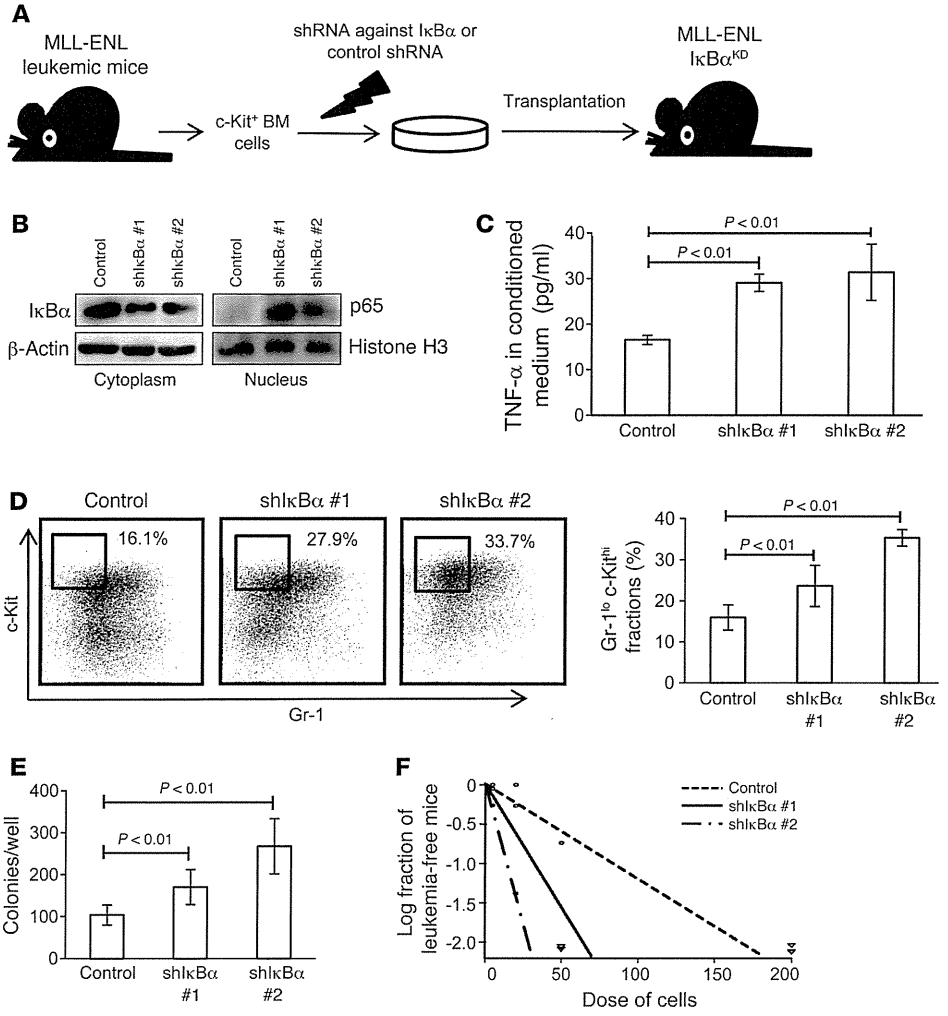

Figure 6
Forcible maintenance of NF-κB activity in leukemia cells enhances LIC frequency. (**A**) Schematic representation of the experiments. c-Kit+ BM cells isolated from MLL-ENL leukemic mice were transduced with shRNA against IκBα or control shRNA and transplanted into sublethally irradiated mice. (**B**) Immunoblotting of cytoplasmic IκBα and nuclear p65 in BM mononuclear cells from MLL-ENL-IκBα^{KD} mice compared with those from control leukemic mice. (**C**) TNF-α secretory ability of MLL-ENL-IκBα^{KD} leukemia cells compared with that of control leukemia cells (n = 4 each). Error bars indicate SD. (**D**) Surface marker profiles of MLL-ENL leukemic mice with or without knockdown of IκBα. Representative FACS plots and mean percentages of Gr-1^{lo}c-Kit^{hi} fractions (n = 6 each). (**E**) CFC assay of MLL-ENL leukemia cells with or without knockdown of IκBα (n = 6). Cells were seeded at 500 cells per well. Error bars indicate SD. (**F**) LIC frequency in BM mononuclear cells derived from MLL-ENL-IκBα^{KD} leukemic mice compared with those from control mice as determined by limiting dilution transplantation assay.

In vivo limiting dilution assays. Varying numbers of cells from different populations were transplanted into sublethally irradiated mice and monitored for disease development (see Supplemental Table 1 for the injected cell numbers).

Immunofluorescence and quantification of p65 nuclear translocation. A total of 1 × 10^4 to 5 × 10^4 cells were cytospun onto glass slides. The cells were fixed with 3.7% formaldehyde in PBS for 30 minutes, permeabilized by treatment with 0.2% Triton X in PBS for 10 minutes, and blocked with 1% BSA in PBS for 60 minutes. Then, the slides were incubated with rabbit anti-p65 polyclonal antibody (sc-372; 1:100 dilution; Santa Cruz Biotechnology Inc.) overnight at 4°C, followed by incubation with Alexa Fluor 555 goat anti-mouse IgG (1:250 dilution; Invitrogen) and TO-PRO3 (1:1,000 dilution; Invitrogen) for 90 minutes. For immunofluorescence staining of Kusabira-Orange+ leukemia cells, Alexa Fluor 647 goat anti-mouse IgG (1:250 dilution; Invitrogen) was used as a secondary antibody, and the nucleus was stained with DAPI. After the cells were washed, they were treated with ProLong Gold Antifade Reagent (Invitrogen). Images were acquired using an Olympus FluoView FV10i confocal microscope with a ×60 objective oil immersion lens. The mean intensity of p65 in the nucleus and cytoplasm of each cell was measured within a region of interest (ROI) placed within the nucleus and cytoplasm. Similarly, the background intensity was quantified within an ROI placed outside the cells. All the measurements were performed using FluoView software. The background-subtracted intensity ratio of nucleus/cytoplasm was calculated in more than 50 cells in each specimen, and the average intensity with SD is presented.

Flow cytometry. Isolation of each fraction from normal or leukemic BM cells was performed using a FACSAria II (BD) cell sorter. For isolation of GMPs and KSLs, biotinylated antibodies against Gr-1 (RB6-8C5), CD11b (M1/70), B220 (RA-3-6B2), CD3 (145-2C11), CD4 (GK1.5), CD8 (53-6.7), and TER119 were used for lineage staining. A PerCP-Cy5.5–labeled streptavidin antibody was used for secondary staining, together with APC-anti-c-Kit (2B8), PE-Cy7-anti-Sca-1 (E13-161.7). FITC-anti-CD34 (RAM34), and PE-anti-CD16/32b antibodies (clone 93). The following antibodies were used for isolation of L-GMPs from GFP-containing leukemia cells: APC-Cy7–anti-streptavidin, PE-Cy5–anti-c-Kit (2B8), PE-Cy7–anti-Sca-1 (E13-161.7), Alexa Fluor 647–anti-CD34 (RAM34), and PE–anti-CD16/32b (clone 93). APC-antistreptavidin and PE-Cy7–anti-Sca-1 antibodies (E13-161.7) were used for sorting LICs and non-LICs in the BCR-ABL plus NUP98-HOXA9 leukemia model. See Supplemental Figures 1 and 2 for detailed FACS plots. For analysis of TNF receptor expression in leukemia cells, biotinylated antibodies against TNF receptor I or II (55R-170) and an APC-Cy7–antistreptavidin antibody were used. Analysis was performed using FlowJo software (Tree Star Inc.).

Table 1
Clinical characteristics of the 12 patients with AML and the 5 patients with normal BM findings

Patient no.	Age	Sex	BM findings	Disease status	Type	Cytogenetics	Blast (%)
1	42	M	AML	Untreated	M2	Normal	87
2	62	M	AML	Relapse	M1	47, XY, del(9)(q13q22),+10	96
3	69	M	AML	Untreated	M4	Normal	90
4	58	M	AML	Untreated	M3	46, XY, t(15;17)	63
5	75	M	AML	Untreated	M4	46, XY, inv(16)	27
6	62	F	AML	Untreated	AML-MRC	NA	24.8
7	72	F	AML	Untreated	AML-MRC	Complex	21
8	42	M	AML	Untreated	M4	46, XY, t(11;17)	25
9	66	M	AML	Untreated	M1	46, XY, t(8;21)	85.4
10	73	F	AML	Untreated	AML-MRC	Complex	44.5
11	65	M	AML	Untreated	AML-MRC	46, XY, t(1;3)	53.3
12	73	M	AML	Untreated	M2	46, XY, add(7)	51.5
13	67	F	Normal			Normal	
14	64	F	Normal			Normal	
15	47	F	Normal			Normal	
16	54	M	Normal			Normal	
17	29	M	Normal			Normal	

Real-time quantitative PCR. Real-time quantitative PCR was carried out on the LightCycler480 system (Roche) using SYBR green reagents according to the manufacturer's instructions. The results were normalized to *Gapdh* levels. Relative expression levels were calculated using the 2-ΔΔCt method (51). The following primers were used for real-time PCR experiments: *Gapdh* forward, TGGCCTCCAAGGAGTAAGAA, and reverse, GGTCTGGGATGGAAATTGTG; *Ncf2* forward, CCAGAAGACCTGGAATTTGTG, and reverse, AAATGCCAACTTTCCCTTTACA; *Tnf* forward, TCTTCTCATTCCTGCTTGTGG, and reverse, GGTCTGGGCCATAGAACTGA; *Il15ra* forward, TAAGCGGAAAGCTGGAACAT, and reverse, TGAGGTCACCTTTGGTGTCA; *Litaf* forward, CTCCAGGACCTTACCAAGCA, and reverse, AGGTGGATTCATTCCCTTCC; *Hoxa9* forward, GGTGCCTGCTGCAGTGTAT, and reverse, GTTCCAGCCAGGAGCGCATAT; *Psma5* forward, CGAGTACGACAGGGGTGTG, and reverse, TGGATGCCAATGGCTGTAG; *Psmd4* forward, GTACATGCGGAACGGAGACT, and reverse, TGTGGTCAGCACCTCACAGT; *Psme3* forward, TTTCAGAGAGCGGATCACAA, and reverse, GGTCATGGATATTTAGAATTGGTTC.

siRNA interference. Specific shRNAs targeting murine *Ikba* mRNA were designed and cloned into pSIREN-RetroQ-ZaGreen vectors. Control shRNA is a nonfunctional construct provided by Clontech. The target sequences, from 5′ to 3′, were: CCGAGACTTTCGAGGAAAT (shIκBα number 1), and AGCTGACCCTGGAAAATCT (shIκBα number. 2).

Immunoblotting. Membranes were probed with the following antibodies: anti-IκBα (Cell Signaling Technology), anti-phospho-IκBα (Ser32) (Cell Signaling Technology), anti-p65 (Santa Cruz Biotechnology Inc.), anti-phospho-p65 (Ser536) (Cell Signaling Technology), anti-β-actin (Cell Signaling Technology), and anti-histone H3 (Cell Signaling Technology). Protein levels were quantified with ImageJ software (NIH). To obtain nuclear and cytoplasmic extracts, an Active Motif Nuclear Extract Kit was used according to the manufacturer's instructions. Cycloheximide treatment assay was performed as described previously, with modification (52). Cells were pretreated with MG132 (20 μM) for 1 hour to initially inhibit the proteasomal degradation of IκBα. Cells were washed twice with medium, then cultured with or without 10 μg/ml of cycloheximide for an additional hour and harvested.

CFC assays. In each experiment, cells were plated onto MethoCult GF M3434 medium (STEMCELL Technologies). Colony numbers in each dish were scored on day 7.

Measurement of TNF-α levels in BM extracellular fluid and conditioned media. BM extracellular fluid was obtained by flushing bilateral femurs and tibia of individual mice with 400 μl PBS. The supernatant was collected after centrifugation. To obtain conditioned media, 0.3–1.0 × 10^6 murine leukemia cells or normal GMPs were cultured in RPMI medium containing 10% FBS and 10 ng/ml IL-3. After a 48-hour incubation, the culture supernatants were collected. The concentration of TNF-α was measured using a murine TNF-α ELISA kit (GenProbe Diaclone) according to the manufacturer's instructions. Similarly, 0.5 × 10^4 to 2.0 × 10^4 human AML or normal $CD34^+CD38^-$ cells were cultured for 48 hours in RPMI medium containing 10% FBS and 100 ng/ml SCF, IL-3, and thrombopoietin. The concentration of TNF-α in the harvested supernatants was measured with a human TNF-α Quantikine ELISA kit (R&D Systems).

20S proteasome activity. A 20S proteasome activity assay kit (Cayman Chemical) was used to analyze proteasome activity. A total of 5 × 10^4 freshly isolated normal GMPs, LICs, and non-LICs in each model were assayed according to the manufacturer's protocol. As a control, the proteasome activity of each cell was also assayed after the specific proteasome inhibitor epigallocatechin gallate was added. Fluorescence was measured with a Wallac ARVO V (PerkinElmer), and the proteasome activity of each cell type was calculated by subtracting the respective control value.

Bortezomib treatment studies. For in vivo treatment experiments, LICs of each leukemia model were injected into sublethally irradiated mice: 1 × 10^3 cells in the MLL-ENL or BCR-ABL/NUP98-HOXA9 models, and 1 × 10^4 cells in the MOZ-TIF2 model. Bortezomib was administrated i.p. at doses of 1.0 mg/kg twice weekly for 3 weeks. Treatment was started 1 week after transplantation in the MLL-ENL or BCR-ABL/NUP98-HOXA9 models, and 2 weeks after transplantation in the MOZ-TIF2 model. For experiments analyzing changes in LIC populations, bortezomib was administrated i.p. at doses of 1.0 mg/kg into fully developed leukemic mice. GFP^+ BM cells were collected 24 hours after injection, and surface marker profiles were analyzed.

Analysis of microarray data. We analyzed publicly available gene expression microarray data on murine and human samples from the Gene Expression Omnibus (GEO) database (GEO GSE24797, GSE20377, and GSE24006). A set of CEL files were downloaded from GEO and normalized using the JustRMA function from the Affy package 1.22.1 in Bioconductor. To compare expression profiles of the NF-κB target genes, normalized data were tested for GSEA using previously described NF-κB target gene sets (29), and a nominal *P* value was calculated. For screening of genes with elevated expression levels in LICs compared with those in normal HSPCs, the expression values of individual genes were compared between groups. Genes significantly elevated in LICs from all three leukemia models as determined by an unpaired Student's *t* test ($P < 0.05$)

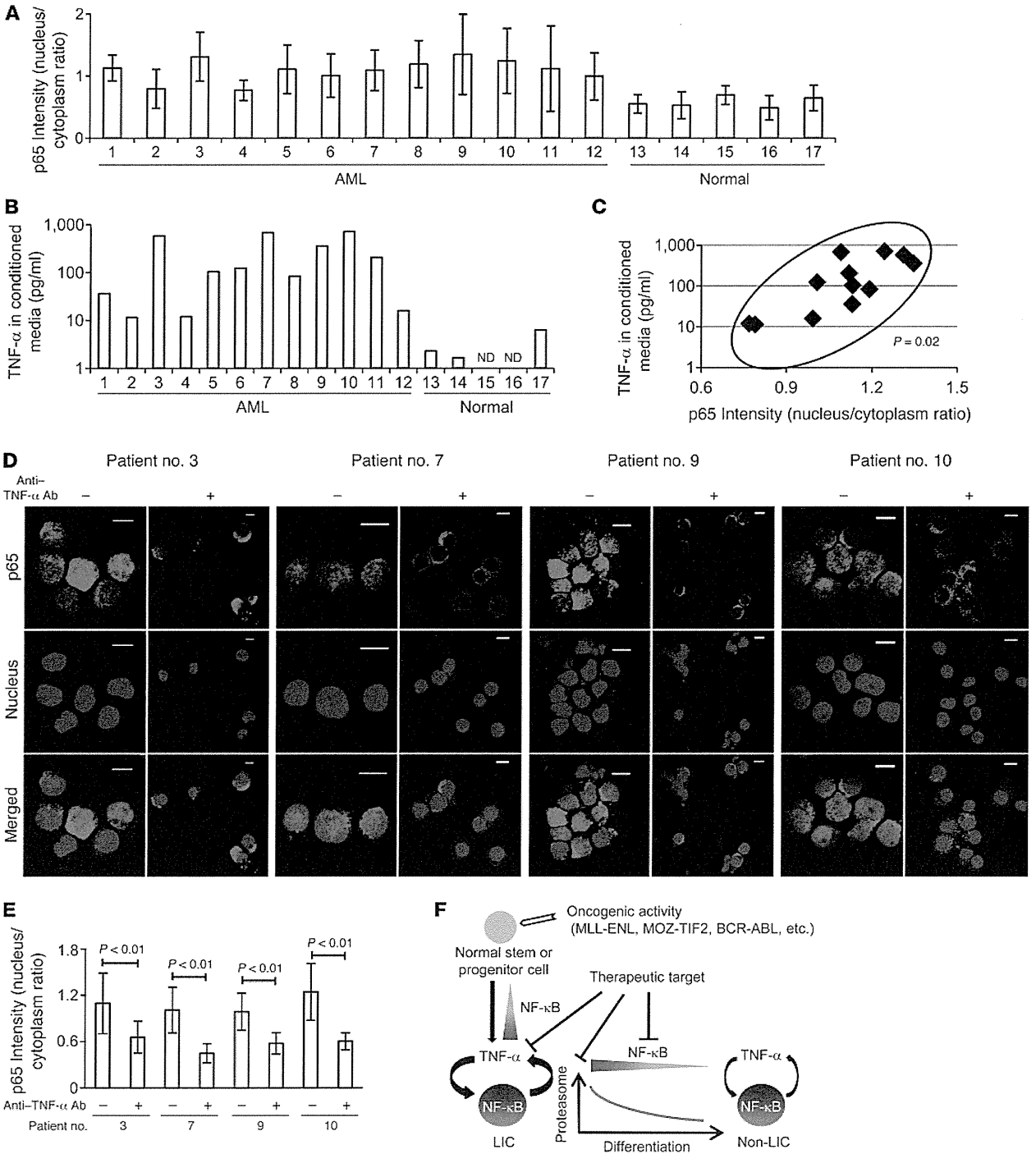

Figure 7

NF-κB/TNF-α positive feedback loop is activated in human AML LICs. (**A**) Quantification of p65 nuclear translocation assessed by the mean nucleus/cytoplasm intensity ratio by immunofluorescence staining. The $CD34^+CD38^-$ fractions isolated from AML or normal BM were analyzed. More than 50 cells were scored in each specimen, and the average intensity ratio with SD is shown. (**B**) TNF-α concentration of culture media conditioned by human AML LICs and normal HSCs measured by ELISA. ND, not detected. (**C**) Correlation between p65 nuclear translocation intensity ratio and TNF-α secretory ability of human AML LICs. (**D**) Immunofluorescence assessment of p65 nuclear translocation in LICs purified from 4 patients after serum-free culture with neutralizing antibody against TNF-α or isotype control. Scale bars: 10 μm. (**E**) Quantification of p65 nuclear translocation of LICs with or without neutralizing antibody against TNF-α assessed by the mean nucleus/cytoplasm intensity ratio. (**F**) Proposed model showing the role of NF-κB signaling in LICs. Positive feedback loop involving NF-κB/TNF-α promotes the maintenance and proliferation of LICs. The signaling is supported by active proteasome machinery, which declines with LIC differentiation.

were selected, among which genes also elevated in human AML LICs (Student's *t* test set at $P < 0.01$) were ultimately selected.

Statistics. Statistical significance of differences between groups was assessed with a 2-tailed unpaired Student's *t* test. Differences were considered statistically significant at a *P* value of less than 0.05. LIC frequency was calculated by Poisson statistics. In leukemia cell transplantation experiments, the overall survival of mice in BM transplantation assays is depicted by a Kaplan-Meier curve. Survival between groups was compared using the log-rank test. To measure the correlation between NF-κB intensity and TNF-α secretion in human AML samples, the Spearman's rank correlation coefficient was used.

Study approval. A total of 12 BM cells derived from patients with AML were obtained from the Department of Hematology and Oncology of the University of Tokyo Hospital. Five BM cells from patients diagnosed with lymphoid neoplasia without BM invasion were used as normal controls. The study was approved by the ethics committee of the University of Tokyo, and written informed consent was obtained from all patients whose samples were collected. All animal experiments were approved by the University of Tokyo Ethics Committee for Animal Experiments.

Acknowledgments

We thank T. Kitamura for the Plat-E packaging cells; H. Nakauchi and M. Onodera for the pGCDNsam-IRES-EGFP retroviral vector; R. Ono and T. Nosaka for the MLL-ENL cDNA; I. Kitabayashi for the MOZ-TIF2 cDNA; W. Hahn for the pBabe-GFP and pBabe-GFP-IκB-SR; and H. Algül and R.M. Schmid for providing the *Rela*-floxed mice. This work was supported by a Grant-in-Aid for Scientific Research A (KAKENHI 12020240) from the Ministry of Education, Culture, Sports, Science and Technology of Japan.

Received for publication December 3, 2012, and accepted in revised form October 17, 2013.

Address correspondence to: Mineo Kurokawa, Department of Hematology and Oncology, Graduate School of Medicine, The University of Tokyo, 7-3-1 Hongo, Bunkyo-ku, Tokyo 113-8655, Japan. Phone: 81.3.5800.9092; Fax: 81.3.5840.8667; E-mail: kurokawa-tky@umin.ac.jp.

1. Bonnet D, Dick JE. Human acute myeloid leukemia is organized as a hierarchy that originates from a primitive hematopoietic cell. *Nat Med.* 1997; 3(7):730–737.
2. Lapidot T, et al. A cell initiating human acute myeloid leukaemia after transplantation into SCID mice. *Nature.* 1994;367(6464):645–648.
3. Ishikawa F, et al. Chemotherapy-resistant human AML stem cells home to and engraft within the bone-marrow endosteal region. *Nat Biotechnol.* 2007; 25(11):1315–1321.
4. Marcucci G, Haferlach T, Döhner H. Molecular genetics of adult acute myeloid leukemia: prognostic and therapeutic implications. *J Clin Oncol.* 2011; 29(5):475–486.
5. Mardis ER, et al. Recurring mutations found by sequencing an acute myeloid leukemia genome. *N Engl J Med.* 2009;361(11):1058–1066.
6. Sen R, Baltimore D. Inducibility of kappa immunoglobulin enhancer-binding protein Nf-κB by a post-translational mechanism. *Cell.* 1986;47(6):921–928.
7. La Rosa FA, Pierce JW, Sonenshein GE. Differential regulation of the c-myc oncogene promoter by the NF-κB rel family of transcription factors. *Mol Cell Biol.* 1994;14(2):1039–1044.
8. Guttridge DC, Albanese C, Reuther JY, Pestell RG, Baldwin AS Jr. NF-κB controls cell growth and differentiation through transcriptional regulation of cyclin D1. *Mol Cell Biol.* 1999;19(8):5785–5799.
9. Duckett CS. Apoptosis and NF-κB: the FADD connection. *J Clin Invest.* 2002;109(5):579–580.
10. Karin M, Greten FR. NF-κB: linking inflammation and immunity to cancer development and progression. *Nat Rev Immunol.* 2005;5(10):749–759.
11. Karin M. Nuclear factor-κB in cancer development and progression. *Nature.* 2006;441(7092):431–436.
12. Pikarsky E, et al. NF-κB functions as a tumour promoter in inflammation-associated cancer. *Nature.* 2004;431(7007):461–466.
13. Guzman ML, et al. Nuclear factor-κB is constitutively activated in primitive human acute myelogenous leukemia cells. *Blood.* 2001;98(8):2301–2307.
14. Guzman ML, et al. Preferential induction of apoptosis for primary human leukemic stem cells. *Proc Natl Acad Sci U S A.* 2002;99(25):16220–16225.
15. Frelin C, et al. Targeting NF-κB activation via pharmacologic inhibition of IKK2-induced apoptosis of human acute myeloid leukemia cells. *Blood.* 2005;105(2):804–811.
16. Carvalho G, et al. Inhibition of NEMO, the regulatory subunit of the IKK complex, induces apoptosis in high-risk myelodysplastic syndrome and acute myeloid leukemia. *Oncogene.* 2007;26(16):2299–2307.
17. Guzman ML, et al. An orally bioavailable parthenolide analog selectively eradicates acute myelogenous leukemia stem and progenitor cells. *Blood.* 2007;110(13):4427–4435.
18. Jenkins C, et al. Nuclear factor-κB as a potential therapeutic target for the novel cytotoxic agent LC-1 in acute myeloid leukaemia. *Br J Haematol.* 2008;143(5):661–671.
19. Jin Y, et al. Antineoplastic mechanism of niclosamide in acute myelogenous leukemia stem cells: inactivation of the NF-κB pathway and generation of reactive oxygen species. *Cancer Res.* 2010;70(6):2516–2527.
20. Takahashi S, et al. Over-expression of Flt3 induces NF-κB pathway and increases the expression of IL-6. *Leuk Res.* 2005;29(8):893–899.
21. Liu S, et al. Sp1/NFκB/HDAC/miR-29b regulatory network in KIT-driven myeloid leukemia. *Cancer Cell.* 2010;17(4):333–347.
22. Nakagawa M, et al. AML1/RUNX1 functions as a cytoplasmic attenuator of NF-κB signaling in the repression of myeloid tumors. *Blood.* 2011; 118(25):6626–6637.
23. Eppert K, et al. Stem cell gene expression programs influence clinical outcome in human leukemia. *Nat Med.* 2011;17(9):1086–1093.
24. Sarry JE, et al. Human acute myelogenous leukemia stem cells are rare and heterogenous when assayed in NOD/SCID/IL2Rγc-deficient mice. *J Clin Invest.* 2011;121(1):384–395.
25. Liu T, et al. Functional characterization of meningioma 1 as collaborating oncogene in acute leukemia. *Leukemia.* 2010;24(3):601–612.
26. Kvinlaug BT, et al. Common and overlapping oncogenic pathways contribute to the evolution of acute myeloid leukemias. *Cancer Res.* 2011; 71(12):4117–4129.
27. Neering SJ, et al. Leukemia stem cells in a genetically defined murine model of blast-crisis CML. *Blood.* 2007;110(7):2578–2585.
28. Wang Y, et al. The Wnt/β-catenin pathway is required for the development ofleukemia stem cells in AML. *Science.* 2010;327(5973):1650–1653.
29. Hinz M, et al. Nuclear factor κB-dependent gene expression profiling of Hodgkin's disease tumor cells, pathogenetic significance, and link to constitutive signal transducer and activator of transcription 5a activity. *J Exp Med.* 2002;196(5):605–617.
30. Gentles AJ, Plevritis SK, Majeti R, Alizadeh AA. Association of a leukemic stem cell gene expression signature with clinical outcomes in acute myeloid leukemia. *JAMA.* 2010;304(24):2706–2715.
31. Kishore N, et al. A selective IKK-2 inhibitor blocks NF-κB-dependent gene expression in interleukin-1 β-stimulated synovial fibroblasts. *J Biol Chem.* 2003;278(35):32861–32871.
32. Algül H, et al. Pancreas-specific RelA/p65 truncation increases susceptibility of acini to inflammation-associated cell death following cerulein pancreatitis. *J Clin Invest.* 2007;117(6):1490–1501.
33. Beg AA, Finco TS, Nantermet PV, Baldwin AS Jr. Tumor necrosis factor and interleukin-1 lead to phosphorylation and loss of IκBα: a mechanism for NF-κB activation. *Mol Cell Biol.* 1993;13(6):3301–3310.
34. DeNardo DG, Coussens LM. Inflammation and breast cancer. Balancing immune response: crosstalk between adaptive and innate immune cells during breast cancer progression. *Breast Cancer Res.* 2007;9(4):212.
35. McLean MH, et al. The inflammatory microenvironment in colorectal neoplasia. *PLoS One.* 2011; 6(1):e15366.
36. Charles KA, et al. The tumor-promoting actions of TNF-α involve TNFR1 and IL-17 in ovarian cancer in mice and humans. *J Clin Invest.* 2009; 119(10):3011–3023.
37. Moore RJ, et al. Mice deficient in tumor necrosis factor-α are resistant to skin carcinogenesis. *Nat Med.* 1999;5(7):828–831.
38. Popivanova BK, et al. Blocking TNF-α in mice reduces colorectal carcinogenesis associated with chronic colitis. *J Clin Invest.* 2008;118(2):560–570.
39. Egberts JH, et al. Anti-tumor necrosis factor therapy inhibits pancreatic tumor growth and metastasis. *Cancer Res.* 2008;68(5):1443–1450.
40. Li J, et al. TNF-α induces leukemic clonal evolution ex vivo in Fanconi anemia group C murine stem cells. *J Clin Invest.* 2007;117(11):3283–3295.
41. Hoang T, Levy B, Ouetto N, Hainan A, Rodriguez-Cimadevilla JC. Tumor necrosis factor α stimulates the growth of the clonogenic cells of acute myeloblastic leukemia in synergy with granulocyte-macrophage colonystimulating factor. *J Exp Med.* 1989;170(1):15–26.
42. Khoury E, et al. Tumor necrosis factor alpha (TNF α) downregulates c-kit proto-oncogene product expression in normal and acute myeloid leukemia $CD34^+$ cells via p55 TNF alpha receptors. *Blood.* 1994;84(8):2506–2514.
43. Zhang B, et al. Altered microenvironmental regulation of leukemic and normal stem cells in chronic myelogenous leukemia. *Cancer Cell.* 2012; 21(4):577–592.
44. Kerbauy DM, Lesnikov V, Abbasi N, Seal S, Scott B, Deeg HJ. NF-κB and FLIP in arsenic trioxide (ATO)-induced apoptosis in myelodysplasticsyndromes (MDSs). *Blood.* 2005;106(12):3917–3925.
45. Adams J. The development of proteasome inhibitors as anticancer drugs. *Cancer Cell.* 2004;5(5):417–421.
46. Chen L, Madura K. Increased proteasome activity,

ubiquitin-conjugating enzymes, and eEF1A translation factor detected in breast cancer tissue. *Cancer Res.* 2005;65(13):5599–5606.
47. Stein SJ, Baldwin AS. Deletion of the NF-κB subunit p65/RelA in the hematopoietic compartment leads to defects in hematopoietic stem cell function. *Blood.* 2013;121(25):5015–5024.
48. Iversen PO, Wiig H. Tumor necrosis factor α and adiponectin in bone marrow interstitial fluid from patients with acute myeloidleukemia inhibit normal hematopoiesis. *Clin Cancer Res.* 2005; 11(19 pt 1):6793–6799.
49. Pronk CJ, Veiby OP, Bryder D, Jacobsen SE. Tumor necrosis factor restricts hematopoietic stem cell activity in mice: involvement of 2 distinct receptors. *J Exp Med.* 2011;208(8):1563–1570.
50. Taniguchi T, Takata M, Ikeda A, Momotani E, Sekikawa K. Failure of germinal center formation and impairment of response to endotoxin in tumor necrosis factor alpha-deficient mice. *Lab Invest.* 1997; 77(6):647–658.
51. Schmittgen TD, Livak KJ. Analyzing real-time PCR data by the Comparative C(T) method. *Nat Protoc.* 2008;3(6):1101–1108.
52. Jain AK, Bloom DA, Jaiswal AK. Nuclear import and export signals in control of Nrf2. *J Biol Chem.* 2005;280(32):29158–29168.

Int J Hematol (2013) 98:206–213
DOI 10.1007/s12185-013-1399-4

ORIGINAL ARTICLE

Unrelated allogeneic bone marrow-derived mesenchymal stem cells for steroid-refractory acute graft-versus-host disease: a phase I/II study

Kazuo Muroi · Koichi Miyamura · Kazuteru Ohashi · Makoto Murata · Tetsuya Eto · Naoki Kobayashi · Shuichi Taniguchi · Masahiro Imamura · Kiyoshi Ando · Shunichi Kato · Takehiko Mori · Takanori Teshima · Masaki Mori · Keiya Ozawa

Received: 27 May 2013 / Revised: 5 July 2013 / Accepted: 9 July 2013 / Published online: 17 July 2013

Abstract We conducted a multicenter phase I/II study using mesenchymal stem cells (MSCs) manufactured from the bone marrow of healthy unrelated volunteers to treat steroid-refractory acute graft-versus-host disease (aGVHD). Fourteen patients with hematological malignancies who suffered from grade II (9 patients) or III aGVHD (5) were treated. Affected organs were gut (10 patients), skin (9 patients), and liver (3 patients). Seven patients had two involved organs. The median age was 52. No other second-line agents were given. MSCs were given at a dose of 2×10^6 cells/kg for each infusion twice a week for 4 weeks. If needed, patients were continuously given MSCs weekly for an additional 4 weeks. By week 4, 13 of 14 patients (92.9 %) had responded to MSC therapy with a complete response (CR; $n = 8$) or partial response (PR; $n = 5$). At 24 weeks, 11 patients (10 with CR and 1 with PR) were alive. At 96 weeks, 8 patients were alive in CR. A total of 6 patients died, attributable to the following: underlying disease relapse (2 patients), breast cancer relapse (1), veno-occlusive disease (1), ischemic cholangiopathy (1), and

K. Muroi (✉)
Division of Cell Transplantation and Transfusion, Jichi Medical University Hospital, 3311-1 Yakushiji, Shimotsuke, Tochigi 329-0498, Japan
e-mail: muroi-kz@jichi.ac.jp

K. Miyamura
Department of Hematology, Japanese Red Cross Nagoya First Hospital, Nagoya, Japan

K. Ohashi
Hematology Division, Tokyo Metropolitan Komagome Hospital, Tokyo, Japan

M. Murata
Department of Hematology and Oncology, Nagoya University Graduate School of Medicine, Nagoya, Japan

T. Eto
Department of Hematology, Hamanomachi Hospital, Fukuoka, Japan

N. Kobayashi
Department of Internal Medicine, Sapporo Hokuyu Hospital, Sapporo, Japan

S. Taniguchi
Department of Hematology, Toranomon Hospital, Tokyo, Japan

M. Imamura
Department of Hematology, Hokkaido University Graduate School of Medicine, Sapporo, Japan

K. Ando
Division of Hematology/Oncology, Department of Internal Medicine, Tokai University School of Medicine, Isehara, Japan

S. Kato
Department of Cell Transplantation and Regenerative Medicine, Tokai University School of Medicine, Isehara, Japan

T. Mori
Division of Hematology, Keio University School of Medicine, Tokyo, Japan

T. Teshima
Center for Cellular and Molecular Medicine, Kyushu University Graduate School of Medicine, Fukuoka, Japan

M. Mori · K. Ozawa
Division of Hematology, Jichi Medical University, Shimotsuke, Japan

pneumonia (1). No clear adverse effects associated with MSC infusion were observed. Third party-derived bone marrow MSCs may be safe and effective for patients with steroid-refractory aGVHD.

Keywords Mesenchymal stem cells · GVHD · Steroid

Introduction

Allogeneic hematopoietic stem cell transplantation (AlloHSCT) is a curative therapy for hematological malignancies and hemopoietic stem cell disorders. Acute graft-versus-host disease (aGVHD), the most important complication associated with AlloHSCT, develops in a significant number of patients who receive AlloHSCT despite GVHD prophylaxis [1]. Levine et al. [2] showed using Cox regression analysis that GVHD grade had a significant impact on non-relapse mortality and overall survival (OS) in a phase II GVHD treatment trial. The relative risk of non-relapse mortality was 1.72 for patients with grade III–IV GVHD, compared to patients with grade 0–II GVHD. Significant factors on OS were aGVHD grade (0–II versus III–IV), donor type (related versus unrelated), and stem cell source (peripheral blood versus bone marrow versus cord blood).

In general, a steroid is first given to patients with aGVHD; however, about half of the patients do not respond to the therapy [3]. Unfortunately, second-line agents have not clearly shown effectiveness against steroid-refractory aGVHD, because they act as a non-specific immunosuppressant and reduce host immunity, leading frequently to infections caused by bacteria, fungi and viruses [4, 5]. Indeed, most patients with steroid-refractory aGVHD die of aGVHD itself, organ damage, and infections even if such second-line therapy is conducted. Recently, the American Society of Blood and Marrow Transplantation evaluated 29 studies in which agents were administered as secondary therapy in aGVHD [6]. Evaluated agents included mycophenolate mofetil, daclizumab, alemtuzumab, infliximab, etanercept, horse antithymocyte globulin, and so on, but excluded mesenchymal stem cells (MSCs). Importantly, the evaluation of complete response (CR) rates, overall response (OR) rates, and 6-month survival estimates did not support the choice of any specific agents for second-line therapy in aGVHD. Therefore, a new agent for steroid-refractory aGVHD is desirable.

MSCs have unique characteristics: specific immunosuppressive properties, no immunogenicity on its own, supportive activity for hemopoiesis, and differentiation abilities into fat cells, chondrocytes, and osteoblasts. Since the first dramatic report by LeBlanc et al., there have been several reports on the effectiveness of MSCs against steroid-refractory aGVHD [7–20]. However, there are several problems when evaluating MSCs against steroid-refractory aGVHD in these studies: before MSC administration, patients have already received one or more immunosuppressants other than for GVHD prophylaxis to steroid-refractory aGVHD and the follow-up time of the patients who received MSCs was relatively short. The source of MSCs used for steroid-refractory aGVHD in these studies was heterogeneous: HLA-identical siblings, HLA-haploidentical related donors, and HLA-mismatched unrelated (third-party) donors. The production of MSCs in different institutes leads to concern about purity and cell function. We report a phase I/II trial on steroid-refractory aGVHD using third party-derived bone marrow MSCs. Before MSC administration, patients only received steroids for aGVHD as a first-line therapy.

Materials and methods

Patients

During the period from January 2009 and November 2010, 14 patients were enrolled in a phase I/II trial using third party-derived bone marrow MSCs for steroid-refractory aGVHD across major transplant centers in Japan. This trial, sponsored by JCR Pharmaceuticals Co., Ltd (Ashiya, Japan) and designated JR-031-201, was approved by the ethics committee in each participating facility. Informed consent was obtained from all the patients.

The eligibility requirements included patients with steroid-refractory grade II to IV aGVHD and age over 6 months. Steroid-refractory aGVHD was defined as progression of aGVHD for 3 days with standard-dose steroid administration or no change in aGVHD for 5 days with the therapy. The standard steroid dose (prednisolone or methylprednisolone) was 1–2 mg/kg. Exclusion criteria were as follows: chemorefractory disease, severe infection, positive results of viral infections including human immunodeficiency virus, human T-lymphotropic virus type I, hepatitis B virus, and hepatitis C virus, severe organ damage including heart, lung, kidney, and liver except liver GVHD, uncontrolled hypertension, oxygen saturation at a steady state less than 94 %, and new immunosuppressive agents added other than steroids for aGVHD. In cases where attending physicians did not predict early relapse after AlloHSCT, no remission in acute leukemia, myelodysplastic syndrome, or hematological malignancies was included. All patients received prophylaxis against GVHD with a calcineurin inhibitor (tacrolimus or cyclosporine) alone or a combination of a calcineurin inhibitor and methotrexate or mycophenolate mofetil. The source of hemopoietic stem cell transplants was bone marrow, peripheral blood stem cells, or cord blood. Conditioning

was either myeloablative conditioning such as total body irradiation-based and intravenous busulfan-based regimens or non-myeloablative conditioning such as fludarabine-based regimens. aGVHD was defined according to the 1994 Consensus Conference on Acute GVHD Grading [21].

MSCs

MSCs were manufactured by JCR based on a license from Osiris Therapeutics Inc (Columbia, Merryland, USA) and named JR-031. JR-031 is almost the same as Prochymal produced by Osiris [12, 17]. Briefly, an aliquot of bone marrow obtained from healthy volunteers was cultured in a medium supplemented with 10 % fetal bovine serum from New Zealand (Life Technologies, New York, USA). The fetal bovine serum products were free of bacteria, viruses, mycoplasma, and endotoxins in the checking tests. The products met standards for Code of Federal Regulations 9CFR113.53 and the United States Department of Agriculture. Adherent cells were expanded by culture and used as MSCs. Before freezing, cells were examined in the terms of MSC characteristics [22]. Isolated cells showed positivity for CD73, CD90, CD105, and CD166 and negativity for CD34, CD45, and HLA-DR. The cells inhibited the mixed-lymphocyte reaction and differentiated to fat cells, chondrocytes, and osteoblasts. The cells had the ability to produce prostaglandin E2. Multicolor-fluorescence in situ hybridization showed that the cells had no chromosomal abnormalities. No infectious agents such as bacteria, mycoplasma, or viruses were detected in the supernatants of the cells or the cells themselves. No endotoxin was detected in the supernatant.

Treatment schedule and evaluation

Initially, patients received a dose of 2×10^6 MSCs/kg twice a week for 4 weeks. The first infusion of MSCs was given within 48 h of the diagnosis of steroid-refractory aGVHD. The interval between each MSC infusion was 3 or 4 days. The volume of one bag of JR-031 was 15 ml containing 100×10^6 MSC, 1.5 g DMSO, 750 mg of human albumin, and other electroride elements. A solution of 25 ml saline was added to thawed MSCs and they were infused at a speed of around 4 ml/min. Before infusion, either 100–200 mg of hydrocortisone or 5–10 mg of chlorpheniramine or both were given to prevent an infusion reaction. During the total course of MSC infusions, no increase in the dose of immunosuppressants given for GVHD prevention was allowed. As for the steroid dose for GVHD treatment, no increase of more than the initial dose of steroid was allowed. Steroid dose reduction including the start of tapering timing and the reduction dose was left to the physicians who took care of the patient.

Response to aGHVD was evaluated for each involved organ. CR was defined as the complete resolution of aGVHD; partial response (PR), as a decrease in organ stages of aGVHD; no response (NR), as no change in aGVHD; progression (PG), as progressive worsening of aGVHD; mixed response (MR), as a mixture of a decrease and increase in organ stages of aGVHD. Patients were dropped out of this JR-031-201 trial if there was PG after the infusion of 3 doses of MSCs or NR after the infusion of 5 doses of MSCs. After completing MSC infusion for 4 weeks, i.e., 8 doses of MSCs, the response was evaluated. When patients showed PR or MR, 2×10^6 MSCs/kg were further given weekly for 4 weeks. The response of MSC therapy to aGVHD was evaluated as follows: CR or PR by the end of 4, 12, and 24 weeks from the first MSC infusion, as wells as continuous CR for more than 28 days. Other evaluable factors associated with MSC therapy were survival, disease relapse, infection, chronic GVHD, and so on.

Monitoring of adverse effects

To monitor adverse effects associated with MSC therapy, laboratory studies, electrocardiogram (ECG), chest X-ray, and computed tomography (CT) of the chest and abdomen were done according to the schedule; ECG was conducted before the first MSC infusion, at 4, 12, and 24 weeks (the cessation of the study) from the first MSC infusion. Chest X-ray was performed before the first MSC infusion, at 4 and 24 weeks. CT was conducted before the first MSC infusion and at 24 weeks. Vital signs, including percutaneous oxygen saturation concentration, were measured before and after each MSC infusion.

Long-term follow-up

After completing JR-031-201, a long-term follow-up study, JR-031-202, was conducted. The observation period was from the week following the end of JR-031-201, i.e., 25 weeks after the first MSC infusion, to 96 weeks (2 years). Informed consent was obtained from each patient. Evaluated valuables included adverse effects associated with MSC therapy such as the status of aGVHD, development of chronic GVHD (cGVHD), disease relapse, ectopic tissue formation, and so on.

Statistical analysis

Survival was described as time from the first MSC infusion and calculated by the Kaplan–Meier method.

Results

Table 1 shows the characteristics of the patients who received MSCs. The median age was 52 years (range 4–62 years). Thirteen patients were adults, while only one was a child. All patients had hematological malignancies as follows: acute myeloid leukemia, 4 patients; acute lymphoblastic leukemia, 3; myelodysplastic syndrome, 3; chronic lymphocytic leukemia, 1; follicular lymphoma, 1; multiple myeloma, 1; and juvenile myelomonocytic leukemia, 1. Of these, 2 patients (no. 4 and 10) had MLL-related leukemia due to chemotherapy for breast cancer. Breast cancer in both patients was in complete remission before AlloHSCT. No patients with refractory disease to chemotherapy were included. Most patients received a transplant from HLA-mismatched unrelated donors after myeloablative or non-myeloablative conditioning. The source of hematopoietic stem cells for transplantation was bone marrow (9 patients), peripheral blood stem cells (1), and cord blood (4). HLA disparity was shown in the eight pairs. All except 3 patients received a combination of a calcineurin inhibitor and methotrexate as GVHD prophylaxis. All patients were first given either prednisolone or methylprednisolone to treat acute GVHD.

Table 2 shows the aGVHD severity and organ involvement before the first MSC infusion and response to aGVHD. The grade of aGVHD was grade II (9 patients) and III (5 patients). Grade IV aGVHD was not enrolled. The most affected organs were the skin (9 patients) and gut (10 patients). Seven patients had two involved organs. MSCs were first infused on the median 47 days after AlloHSCT. The median number of MSC infusions was eight. By 4 weeks after the first MSC infusion, 8 and 5 patients had achieved CR and PR, respectively. The OR rate was 92.9 % (13 of 14 patients). By 24 weeks, 4 of 5 patients with PR achieved CR. At 96 weeks, 8 patients were alive and in CR. As shown in Fig. 1, the estimated time to reach 50 % CR after the first MSC infusion was 3 weeks (MSC infusion six times). There was no difference in the time to reach CR between grade II and grade III aGVHD (data not shown). Relapse of aGVHD after MSC therapy occurred in one patient (no. 12). At 78 days after the first MSC infusion, he was admitted again because of bloody diarrhea. Endoscopic biopsy showed aGVHD in the cecum and colon. The patient was put on parenteral hyperalimentation with tacrolimus administration. His aGVHD gradually disappeared.

By the end of the follow-up (2 years), 6 patients had died (Table 2). Five of the 6 patients (no. 2, 3, 4, 9, and 10) died due to factors not directly related to aGVHD as follows: no. 9 patient, veno-occlusive disease on day 25; no. 7, hepatic failure on day 36; no. 2, pneumonia on day 82; no. 3 and 10, disease relapse on days 191 and 696, respectively; and no. 4, metastatic breast cancer on day

Table 1 Patient characteristics

Case no.	Age	Sex	Disease	HSCT				GVHD prophylaxis	First line therapy for acute GVHD
				Source	Donor	HLA disparity	Conditioning		
1	56	F	MDS/RCMD	BM	Unrelated	7/8	Myeloab	CyA + sMTX	mPSL
2	59	F	AML/2nd CR	BM	Unrelated	8/8	Myeloab	CyA	mPSL
3	44	M	AML/1st CR	BM	Unrelated	7/8	Myeloab	FK506	mPSL
4	36	F	ALL/2nd Rel	BM	Unrelated	6/8	Myeloab	FK506	mPSL
5	57	F	FL	PB	Sibling	8/8	Myeloab	CyA + sMTX	PSL
6	42	F	ALL/1st CR	BM	Unrelated	8/8	Myeloabl	FK506 + sMTX	PSL
7	29	M	MDS/RAEB	CB	Unrelated	4/8	Myeloab	FK506 + sMTX	mPSL
8	62	F	CLL/PR	CB	Unrelated	5/8	Non-myeloab	FK506 + sMTX	mPSL
9	55	M	ALL/1st CR	BM	Unrelated	8/8	Myeloab	CyA + sMTX	mPSL
10	49	F	AML/1st CR	BM	Unrelated	6/8	Myeloab	FK506 + sMTX	mPSL
11	4	M	JMML/1st CP	CB	Unrelated	5/6	Myeloab	CyA + sMTX	PSL
12	61	M	AML-MRC[a]	CB	Unrelated	4/6	Myeloab	FK506 + MMF	PSL
13	35	F	MM/1st CR	BM	Unrelated	8/8	Non-myeloab	FK506 + sMTX	PSL
14	61	F	MDS/RAEB	BM	Sibling	6/6	Non-myeloab	CyA + sMTX	PSL

HSCT hemopoietic stem cell transplantation, *GVHD* graft-versus-host disease, *F* female, *M* male, *MDS* myelodysplastic syndrome, *RCMD* refractory cytopenia with multilineage dysplasia, *AML* acute myeloid leukemia, *AML-MRC* acute myeloid leukemia with myelodysplasia-related changes, *ALL* acute lymphoblastic leukemia, *FL* follicular lymphoma, *RAEB* refractory anemia with excess of blasts, *CLL* chronic lymphocytic leukemia, *MM* multiple myeloma, *CR* complete remission, *PR* partial remission, *Rel* relapse, *BM* bone marrow, *PB* peripheral blood stem cell, *CB* cord blood, *Myeloab* myeloablative, *Non-myeloab* non-myeloablative, *CyA* cyclosporine, *FK506* tacrolimus, *sMTX* short-term methotrexate, *PSL* prednisolone, *mPSL* methylprednisolone

[a] No chemotherapy before HSCT

Table 2 GVHD and outcome

Case	GVHD				1st MSC infusion	No. of MSC infusions	Response		Survival/ death	Cause of death (days)
	Grade	Skin	Liver	Gut	Days after HSCT		By 4 weeks	By 24 weeks	At 96 weeks	
1	II	3	0	0	38	8	PR	PR	Alive in CR	N/A
2	II	1	0	1	50	10	PR	CR	Dead	Pneumonia (82)
3	II	3	0	0	43	12	PR	CR	Dead	Relapse (696)
4	III	1	0	2	51	12	CR	CR	Dead	Breast cancer (244)
5	II	3	0	1	46	8	CR	CR	Alive in CR	N/A
6	II	3	0	0	48	8	CR	CR	Alive in CR	N/A
7	III	0	1	2	33	5	PG	–	Dead	IC (36)
8	III	3	0	3	57	12	PR	CR	Alive in CR	N/A
9	II	1	0	1	38	3	CR	CR	Dead	VOD (25)
10	II	0	0	1	45	8	CR	CR	Dead	Relapse (191)
11	III	0	2	4	78	12	PR	CR	Alive in CR	N/A
12	II	0	1	0	52	8	CR	CR	Alive in CR	N/A
13	III	3	0	4	44	8	CR	CR	Alive in CR	N/A
14	II	0	0	1	108	7	CR	CR	Alive in CR	N/A

GVHD graft-versus-host disease, *MSC* mesenchymal stem cell, *HSCT* hemopoietic stem cell transplantation, *CR* complete response, *PR* partial response, *PG* progression, *VOD* veno-occlusive disease, *IC* ischemic cholangiopathy, *N/A* not applicable

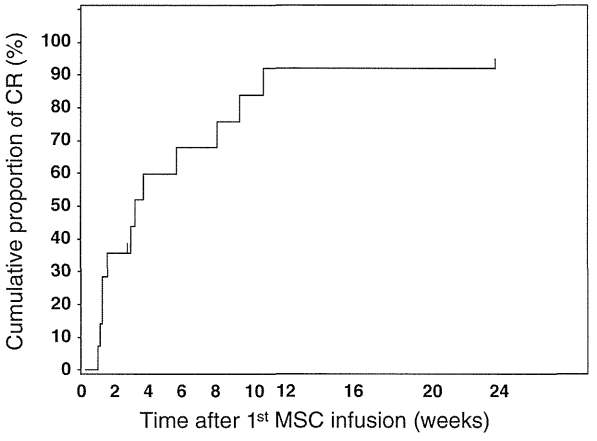

Fig. 1 Time to achieve complete response

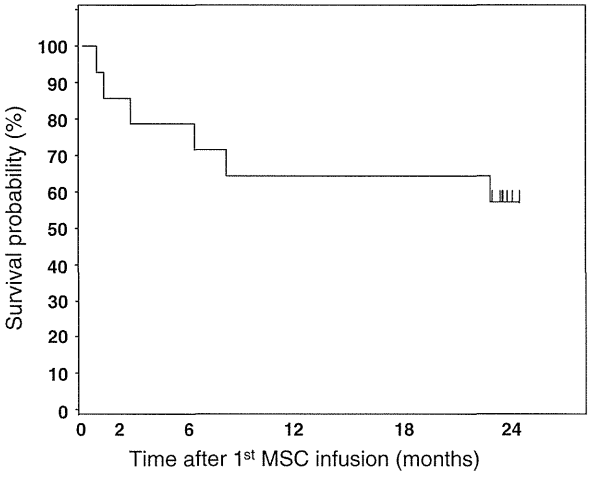

Fig. 2 Overall survival

244. The no. 2 patient showed pancytopenia caused by ganciclovir treatment for CMV antigenemia and died of pneumonia with massive pleural effusion. Autopsy findings showed pulmonary aspergillosis. Two patients with acute myeloid leukemia (no. 3 and 10) relapsed; the former received a second bone marrow transplant from another donor, but he died of sepsis. The latter died of septic shock after chemotherapy for disease relapse. Patient no. 4 maintained CR after MSC therapy, but a scheduled CT scan incidentally showed multiple low-density areas in both liver lobes on day 145. A liver biopsy demonstrated adenocarcinoma, leading to the suspicion of liver metastasis of breast cancer. Bone scintigraphy showed multiple isotope uptake regions in vertebrae and pelvic bone. The patient was diagnosed with recurrent breast cancer in the liver and bone and died of breast cancer. Patient no. 7 was evaluated as having PG of aGVHD. Serum liver enzyme levels and bilirubin values progressively worsened, leading to death. Necropsy of the liver showed ischemic cholangiopathy characterized by massive hepatocyte necrosis, marked congestion in the bile ducts, hyaline degeneration in the arterioles, disappearance of endothelial cells in the arterioles, and slight infiltration of lymphocytes. OS is shown in Fig. 2. There was no

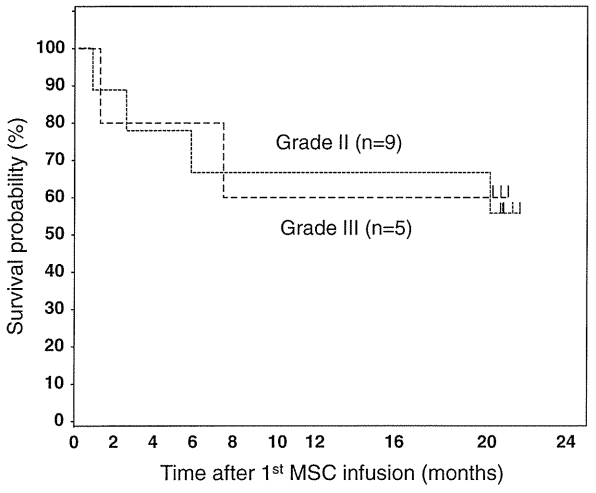

Fig. 3 Overall survival in the category of grade II and III acute GVHD. There was no difference between the two groups

difference in survival between groups of patients with grade II and grade III aGVHD (Fig. 3).

Adverse effects associated with MSC therapy were monitored. No infusion toxicity such as fever or decrease in oxygen saturation was observed. In the JCR-031-201 study, 27 events of infection episodes in 13 patients were collected as follows: bacteremia (3 events, 3 patients), pneumonia (4, 3), herpes zoster (3, 2), oral candidiasis (2, 2), infectious enterocolitis (2, 2), CMV antigenemia (2, 2), sepsis (1, 1), CMV colitis (1, 1), hemorrhagic cystitis (1, 1), and others (7, 7). In the JCR-031-202 study, 28 events in 9 patients were collected as follows: pneumonia (3 events, 3 patients), septic shock (3, 2), sinusitis (2, 2), upper respiratory tract infection (2, 2), oral herpes (4, 2), herpes zoster (1, 1), varicella (1, 1), infectious enterocolitis (1, 1), CMV antigenemia (1, 1), and others (8, 8). Ectopic tissue formation was not detected by scheduled CT scans. cGVHD developed in 7 patients; 4 patients (no. 8 at 24 weeks, 11 at 24 weeks, 12 at 48 weeks, and 14 at 36 weeks) with a limited form, and 3 patients (no. 1 at 24 weeks, 3 at 24 weeks, and 6 at 24 weeks) with an extensive form, of cGVHD.

Discussion

Reports of bone marrow MSCs used for steroid-refractory aGVHD are divided into two approaches; one approach used MSCs produced in the institution where patients were scheduled to receive the cells, while the another used MSCs manufactured in a company. In the former, the largest study was a phase II study conducted by the European Group for Blood and Bone Marrow [11]. Fifty-five patients with a median age of 22 years received MSCs for steroid-refractory aGVHD. Most patients had grade III or IV aGVHD. MSC donors were either HLA-identical, haploidentical, or HLA-mismatched unrelated donors. The median time from aGVHD onset to the first MSC infusion was 25 days. Of note, 33 patients had already received second-line therapy for aGVHD before MSC administration. Most patients received MSCs at a median dose of 1.4×10^6 MSCs/kg once or twice. The overall response rate was 71 % (CR, 30; PR, 9 patients). Twenty-four of these responders received MSCs from third-party donors. The overall estimated 2-year survival in this trial was 35 % and was significantly better in complete responders (53 %) versus non-complete responders (16 %). There was a better trend for 2-year estimated survival in the pediatric population compared to adults. No severe–adverse effects associated with MSC infusions were reported. Except for the report from the European Group for Blood and Bone Marrow, other reports were small-sized clinical studies including a phase I or a phase I/II study to treat steroid-refractory aGVHD with MSCs [7–10, 13–16, 18–20]. Importantly, in all of these studies, any second- or third-line immunosuppressive agent in combination with MSCs was allowed. Therefore, it is difficult to exactly evaluate the effects of MSCs on steroid-refractory aGVHD.

MSCs manufactured by Osiris, Prochymal, were given to steroid-refractory GVHD patients. Kebriaei et al. compared a dose of 2×10^8 Prochymal cells/kg with 8×10^8 Prochymal cells/kg in combination with steroids to treat patients with de novo aGVHD. Thirty-one patients were evaluated: there was no difference between the two groups in terms of safety and efficacy [12]. Prasad et al. [17] showed the efficacy of Prochymal for pediatric patients with severe refractory aGVHD. Most patients received Prochymal at a dose of 2×10^8 cells/kg. Following positive results in these two studies, Osiris conducted a phase III trial investigating Prochymal for steroid-refractory aGVHD across transplant centers in the United States, Canada, and Australia [23]. This was a double-blind placebo-controlled study. Patients were randomized at a 2:1 ratio for either Prochymal or the placebo. The dose of Prochymal was 2×10^8 cells/kg. Of note, most patients had already received a second-line therapy before MSC therapy. This trial enrolled 260 patients. The primary endpoint was durable CR for 28 days. The preliminary analysis did not show a statistical difference between Prochymal and the placebo for the primary endpoint (Prochymal 35 % versus placebo 30 %). However, subpopulation analysis showed that Prochymal significantly improved the response in liver aGVHD (76 versus 47 %) and gastrointestinal aGVHD (82 versus 68 %). Infection rates were not different between the two groups. Rates of severe–adverse effects associated with MSC administration were not different in the two arms. Now, Prochymal is approved for use